HIV-1 RNA genomes initiate host protein packaging in the cytosol independently of Gag capsid proteins

Jordan T. Becker[1#], Edward L. Evans III[1], Bayleigh E. Benner[1], Stephanie L. Pritzl[1], Laura E. Smith[1], Andra E. Bates[1], and Nathan M. Sherer[1*]

[1] McArdle Laboratory for Cancer Research, Institute for Molecular Virology, and Carbone Cancer Center, University of Wisconsin-Madison, Madison, WI, 53706, US

* To whom correspondence should be addressed. Nathan M. Sherer, Tel: +1-608-890-2551; Fax: +1-608-262-2824; Email: nsherer@wisc.edu

#Present Address: Jordan T. Becker, Institute for Molecular Virology, University of Minnesota-Twin Cities, MN, 55455, USA

ABSTRACT

HIV-1 RNA genomes interact with diverse RNA binding proteins (RBPs) in the cytoplasm including antiviral factor APOBEC3G (A3G) that, in the absence of viral Vif proteins, is packaged into virions. Where and when HIV-1-A3G interactions are initiated for packaging inside the cell is unknown, and the relative contributions of genome vs. Gag capsid proteins to this process remains controversial. Here we visualized A3G responses to HIV-1 infection over an entire replication cycle using long-term (up to 72 h) live single cell imaging. We show that Vif-deficient HIV-1 dramatically shifts A3G and a second RNA surveillance factor, MOV10, from the cytoplasm to virus particle assembly sites with little

22 to no net discernible effects on general markers of cytoplasmic processing bodies
23 (DCP1A), stress granules (TIA-1), or a marker of the nonsense-mediated decay
24 machinery (UPF1). Using a new live cell RNA-protein interaction assay based on RNA
25 tethering (the in-cell RNA-protein interaction protocol, or IC-IP), we provide evidence that
26 A3G- and MOV10- genome interactions are selective, strong, occur in presence or
27 absence of Gag, and are initiated in the cytosol soon if not immediately after genome
28 nuclear export. Finally, although Gag is sufficient to package A3G into virions even in the
29 absence of genomes, single virion imaging indicates that selective A3G-genome
30 interactions promote much more consistent per virion delivery of A3G to assembly sites.
31 Collectively, these studies suggest a paradigm for early, strong, and persistent cytosolic
32 detection of select HIV-1 RNA signatures by A3G, MOV10 and other host RBPs that are
33 enriched in virions.

34

35 **IMPORTANCE**

36 Host-pathogen interactions determine the success of viral replication. While extensive
37 work has identified many interactions between HIV-1 and cellular factors, our
38 understanding of where these interactions in cells occur during the course of infection is
39 incomplete. Here, we show that multiple RNA-binding proteins (including the antiviral
40 restriction factor, APOBEC3G, and MOV10 helicase) bind HIV-1 RNA genomes in the
41 cytoplasm and co-traffic with them into progeny virions. Furthermore, we show that these
42 interactions with HIV-1 RNA occur in the absence of Gag and are sufficiently strong to
43 recruit these to otherwise non-native subcellular locales. Together, these data begin to

44 illuminate the intracellular trafficking pathways shared by host RNA binding proteins and

45 the viral RNAs they preferentially bind.

46

47 **INTRODUCTION**

48 The human immunodeficiency virus type 1 (HIV-1) hijacks a diverse set of host
49 cellular RNA binding proteins (RBPs) to carry out viral RNA transcription, nuclear export,
50 translation, and trafficking (1–4). Select host RBPs are packaged into virions and exhibit
51 antiviral properties, with the best-characterized example being members of the
52 Apolipoprotein B mRNA editing enzyme, catalytic polypeptide-like 3 (APOBEC3) family.
53 A subset of APOBEC3 proteins (A3F, A3G, and A3H) can be packaged into virions to
54 abolish infectivity by deaminating cytidines on the nascent minus-sense DNA strand of
55 the viral genome, thereby generating G-to-A mutations in the DNA provirus (5–8). During
56 productive infection, however, APOBEC3 proteins are counteracted by viral infectivity
57 factor (Vif) proteins that facilitate their proteasome-mediated degradation prior to the
58 onset of virus particle production (9–11). Additional host factors that are unaffected by Vif
59 are packaged into virions, some of which, *e.g.*, RNA helicases MOV10 and UPF1, have
60 been implicated as regulatory factors influencing virion infectivity (12–16).

61 How APOBEC proteins evolved to ensure encapsidation into virions remains a
62 poorly understood aspect of the cell-intrinsic host defense. HIV-1 virions are, in essence,
63 transmissible ribonucleoprotein (RNP) complexes, with their assembly driven by viral Gag
64 capsid proteins that multimerize on an RNA scaffold consisting of host-derived RNA
65 molecules and two dimerized viral RNA genomes, with Gag-RNA binding mediated by
66 Gag's C-terminal Nucleocapsid (NC) domain [reviewed in (17, 18)]. In the absence of viral
67 genomes, Gag expression is sufficient to drive formation of non-infectious virus-like
68 particles containing cellular RNAs, packaged in proportion to their relative abundance in
69 the cell (19, 20). A3G's incorporation into virions has been shown, for most cell types, to

70 be both RNA- and NC-dependent (21–26)(22, 27). However, the relative contributions of
71 viral genomes vs. host RNAs to this process remains controversial. On the one hand,
72 A3G can incorporated into virus particles through promiscuous interactions with host RNA
73 even when packageable genomes are not expressed (23, 25, 27). On the other hand,
74 A3G incorporation levels can be enhanced by genomes (16, 21); and A3G exhibits
75 selective RNA-binding characteristics (25, 28) including a reported preference for G-rich
76 segments of the HIV-1 genome (26). One or more additional host factors may contribute
77 to A3G packaging including the 7SL non-coding RNA component of the signal recognition
78 particle (29–32).

79 Where and when A3G and other packaged RBPs interface with Gag and/or
80 genomes in the cell has also been under investigation for some time, with conflicting
81 results. At steady-state, A3G is distributed throughout the cytosol (the aqueous phase of
82 the cytoplasm) and accumulates to high levels at non-membranous cytoplasmic sites of
83 mRNA decay known as processing bodies (PBs) (33, 34). Cytosolic A3G will also rapidly
84 re-localize to sites of translational repression known as stress granules (SGs) in response
85 to heat shock or oxidative stress (33, 34). Although early studies suggested a functional
86 link between PBs and A3G's antiviral activity (34–36); we have not observed viral
87 genomes and Gag to be overtly associated with P bodies (37–39), and dissolution of
88 these structures by depleting P body structural components has no effect on HIV-1
89 replication (37, 40). Because HIV-1 Gag and genomes fill the cytoplasm in a non-localized
90 fashion prior to virion assembly (38, 39, 41, 42), we predicted that the virus-host
91 interactions precipitating A3G packaging were most likely to occur ubiquitously

92 throughout the fluid phase of the cytosol. However, such a scenario has yet to be formally
93 demonstrated.

94 To gain greater understanding of the subcellular dynamics of HIV-1 RNA
95 trafficking, virion production, and host cellular response to infection, herein we carried out
96 a comprehensive analysis of the coordinated behaviors of HIV-1 RNA genomes, Gag,
97 A3G, and markers of PBs, SGs, and the NMD machinery in single cells using single cell
98 video microscopy, in conjunction with a new tethering-based intracellular RNA-protein
99 interaction assay (the in-cell RNA-protein interaction protocol, or IC-IP. Collectively, our
100 results indicate that viral genomes exhibit markedly strong and selective interactions with
101 A3G and at least one additional host RBP, MOV10; that these interactions are Gag-
102 independent; and that these interactions occur throughout the cytosol and are initiated
103 soon if not immediately after viral genome nuclear export.

104

105 **RESULTS**

106 **Single cell imaging using RBP biosensor cell lines to track HIV-1 replication and**
107 **detect host protein packaging.**

108 To study real-time RBP responses to HIV-1 in single cells over an entire round of viral
109 replication, we generated biosensor HeLa cell lines stably expressing fluorescent protein-
110 tagged versions of A3G (YFP-A3G) (Fig. 1A) and, as comparators, cell lines constitutively
111 expressing YFP-MOV10 (Fig. 1I), YFP-UPF1 (a component of the NMD machinery) (Fig.
112 1I), TIA-1-YFP (a marker of SGs) (Fig. 2A) or CFP-DCP1A (a marker of PBs) (Fig. 2E)
113 (33, 63). To address the role(s) of Vif, cells were infected with either Vif-competent (Vif+)
114 HIV-1_{NL4-3} CFP reporter virus or viruses rendered Vif-minus (Vifxx) due to the insertion of
115 two stop codons in the *vif* reading frame (see cartoon depiction in Fig. 1B) (mutation
116 based on ref. (52)). In the absence of infection, YFP-A3G was localized to the cytoplasm
117 and accumulated in bright PBs (Fig. 1A, left panel), with induction of oxidative stress using
118 250 μM sodium arsenite (Ars) causing re-localization of YFP-A3G to SGs, as anticipated
119 (64)(Fig. 1A, right panel). We also confirmed that our YFP-A3G fusion protein was
120 packaged into Vifxx virus particles and retained antiviral activity using single-round
121 assembly and infectivity assays (Fig. 1C).

122 Hela.YFP-A3G cells were infected with Vif+ virus at a MOI of <1 so that infected and
123 uninfected cells would be visualized side-by-side over an entire round of replication,
124 requiring >48 hours of continuous single cell imaging. Viral gene expression (based on
125 the CFP reporter) was initiated 16-20 hours post-infection (hpi), followed by gradual loss
126 of YFP-A3G from 20-25 hpi consistent with Vif-driven degradation (decay rate of 24.5%
127 per h +/-6.0%; n=33; Fig. 1D, Movie S1, and quantification in Fig. 1E). YFP-A3G was

128 depleted from both diffuse cytosolic and PB pools simultaneously, with levels suppressed
129 to near background with little to no discernible fluctuations to Vif activity after 24h (Fig.
130 1D and Fig. 1E showing kinetics over the entire 48h time course). CFP+ cells ultimately
131 became rounded after 40 hpi, consistent with Vif-induced cell cycle arrest (65, 66) (Fig.
132 1D and Movie S1, see 48 h time point).

133 We next infected HeLa.YFP-A3G cells with Vif-deleted (Vifxx) reporter virus. As
134 expected, YFP-A3G expression was maintained in the cytoplasm and at PBs throughout
135 the entire course of infection, and cell cycle arrest was not observed (Fig. 1F,
136 quantification in Fig. 1E and Movie S2). Strikingly, however, in infected cells much of the
137 YFP-A3G signal coalesced into large, up to 4 μm diameter (based on current resolution)
138 clusters at 30-48 hpi (Fig. 1F, white arrows highlight growing clusters); unlikely to be PBs
139 or SGs due to their proximity to the plasma membrane and real-time observations of
140 cluster release and transfer to neighboring cells (Fig. 1F, 32h time point, and Movie S2).
141 YFP-A3G clusters stained positive for both HIV-1 Gag/Gag-Pol and viral genome
142 (unspliced RNA encoding the *gagpol* reading frame) but not *yfp-a3g* mRNA (negative
143 control) detected using a 4-color combined anti-p24^{Gag} immunofluorescence / RNA
144 fluorescence in situ hybridization (IF/FISH) protocol, thus indicating that the clusters most
145 likely represented YFP-A3G recruited to sites of virus particle assembly (Fig. 1G). Thin
146 section electron microscopy confirmed the presence of clusters of virus particles at the
147 surface of HeLa.YFP-A3G cells at 48 hpi for both Vif+ and Vifxx conditions, consistent
148 with this hypothesis (Fig. 1H).

149 For comparison, we also monitored Vif+ and Vifxx infection in cells expressing
150 YFP-MOV10, a superfamily 1 (SF1) RNA helicase and PB protein that is also efficiently

151 packaged into virions and interacts with RNA but, unlike A3G, is not targeted for
152 proteosomal degradation by Vif (13, 14); and cells stably expressing another YFP-tagged
153 SF1 helicase, UPF1, that plays a key role in NMD and is also packaged into virions (12,
154 67) (Fig. 1I, Fig. S1A, and Movie S3). We observed very similar effects of HIV-1 infection
155 on YFP-MOV10 as for YFP-A3G, with large amounts of signal transferred to large plasma
156 membrane clusters at later time points post-infection; both in the presence or absence of
157 Vif (Figs. 1I, S1B, S1C, and Movie S3). By contrast, YFP-UPF1, that exhibits a diffuse
158 distribution in the cytoplasm, was largely unaffected by HIV-1 (Figs. 1I, S1C, and Movie
159 S3); consistent with it being less efficiently packaged into virions relative to YFP-MOV10
160 (Fig. S1A).

161 Taken together, these experiments validated both YFP-A3G and YFP-MOV10 as
162 proxy biosensors for detecting and monitoring HIV-1 infection, with A3G providing for
163 single cell measurements of Vif-induced A3G degradation and cell cycle arrest; and both
164 YFP-A3G (in the absence of Vif) and YFP-MOV10 allowing for direct detection of HIV-1
165 virus particle assembly and host protein packaging as it occurs.

166

167 **HIV-1 replication has no overall effect on processing bodies or stress granules.**

168 Because A3G and MOV10 are enriched in SGs and PBs (33, 34, 37, 40), to address
169 specificity and determine if there are transitional effects of HIV-1 on SGs and PBs over
170 time we next studied biosensor cell lines expressing YFP-TIA-1 or CFP-DCP1A (Fig. 2);
171 validated markers of SGs and PBs, respectively [reviewed in (63)]. We first confirmed that
172 the YFP-TIA-1 "stress" biosensor formed SGs in response to sodium arsenite treatment
173 (Ars) (Fig. 2A, right panel) or in response to infection by using rhinovirus A16 (RVA16), a
174 positive-strand RNA virus we had studied previously (68) and discovered to cause
175 rampant SG formation as early as 4h post-infection (Fig. 2B and Movie S4). CFP-DCP1A
176 was enriched in bright punctae throughout the cytoplasm consistent with PBs, as
177 expected (Fig. 2E).

178 Unlike for RVA16, neither Vif+ nor Vifxx HIV-1 triggered SG formation in either YFP-
179 TIA-1 or YFP-A3G cells over 48h of continuous imaging, a time window sufficient to
180 encompass an entire round of viral replication (Fig. 2C with quantification in Fig. 2D). HIV-
181 1 also had no discernible effects on PB number or morphology in CFP-DCP1A biosensor
182 cells; with PB number being remarkably consistent and stable for individual cells under
183 all conditions (typically 6-9 PBs per cell, Fig. 2E with quantification in Fig. 2F). Unlike
184 YFP-A3G and YFP-MOV10, neither YFP-TIA-1 or CFP-CDP1A were shifted to the
185 plasma membrane over the imaging time course. Based on these observations, we
186 conclude that despite HIV-1's marked effects on YFP-A3G and YFP-MOV10 as shown in
187 Figure 1, net modulation of PBs or induction of SGs are unlikely to be intrinsic features of
188 the HIV-1 replication cycle.

189 HIV-1 Gag has been reported to inhibit SG formation (69–72), so that we also tested
190 the effects of treating HeLa.YFP-A3G or HeLa.YFP-TIA-1 biosensor cells with sodium
191 arsenite at 31 hpi when NL4-3 Gag expression in HeLa cells is relatively high (*e.g.*, see
192 ref.(66)). Contrary to our expectations, both YFP-A3G and YFP-TIA-1 accumulated in
193 SGs in Ars-treated cells with or without infection, for both Vif+ and Vifxx viruses (Fig. 2G
194 with quantification in Fig. 2H). To localize viral genomes under these conditions, we again
195 performed combined *gagpol* FISH and Gag IF, finding the bulk of the HIV-1 *gagpol* signal
196 markedly co-localized with YFP-A3G in Ars-induced SGs (Fig. 2I, compare YFP-A3G
197 panels to *gagpol* FISH panels). By contrast, the cytoplasmic pool of Gag was largely
198 excluded from these complexes (Fig. 2I, compare YFP-A3G panels to Gag anti-p24
199 panels). SGs are induced after kinase R-mediated phosphorylation of translation initiation
200 factor EIF2A, triggering aggregation of scaffolding proteins TIA-1, TIAR, and G3BP1 in
201 complex with mRNAs bound to translation initiation factors and polysome-associated
202 proteins [reviewed in (63, 73)]. Accordingly, marked co-localization of YFP-A3G viral
203 unspliced RNA in SGs would be consistent with A3G co-trafficking with genomes and/or
204 *gagpol* mRNAs in a cytosolic phase that contains free polysomes.

205

206 **Evidence for strong genome-A3G interactions in the cytosol based on FRAP**

207 In order to be able to directly track genomes and Gag in conjunction with YFP-A3G and
208 YFP-MOV10, we next engineered two-color visible HIV-1 viruses expressing Gag-CFP
209 from "self-tagging" RNA genomes bearing 24 copies of the MS2 RNA binding loop
210 (located in the *gag-pol* open reading frame) and encoding an RFP-tagged MS2
211 bacteriophage (MS2-RFP) coat protein expressed from the viral *nef* locus (Vif+ and Vifxx
212 Gag-CFP/MS2-RFP viruses, see cartoon depictions in Figs. 3A and 3C). When plasmids
213 encoding visible HIV-1 were transfected into cells, Gag-CFP expression allowed for single
214 cell measurement of viral late gene expression, with genomes tracked over time using
215 the MS2-RFP proxy. Expression of Vif+ or Vifxx Gag-CFP/MS2-RFP viruses recapitulated
216 effects seen during infection with CFP reporter viruses (see Fig. 1); including rapid, Vif-
217 dependent down-regulation of YFP-A3G (decay rate = 25.9% per hour +/- 7.0%; n = 31,
218 Fig. 3B, green, with quantification in Figs. 3E and 3F, see also Movie S5) and, for Vif-
219 deficient (Vifxx) conditions, co-clustering of YFP-A3G, MS2-RFP-tagged genomes, and
220 Gag-CFP to assembly sites at the plasma membrane (Fig. 4D, arrows, Movie S6; and
221 see Fig. 4D for an example at higher magnification). Vif-induced YFP-A3G degradation
222 occurred prior to the onset of virus particle assembly (Fig. 3B, compare 2 h and 3 h time
223 points) but >1h after genomes populated the cytoplasm (Fig. 3D, compare 1h and 4h time
224 points). A "Genome only" variant was also generated wherein we mutated the *gag* start
225 codon to abolish Gag synthesis (mutation previously described in ref. (39)) (Fig. 3G). We
226 also generated a version wherein we deleted the Rev response element (RRE) in the
227 second major intron in order to abolish genome nuclear export (see Fig. 5F).

228 Both prior to and during virus particle assembly, Vifxx visible genomes and YFP-
229 A3G were co-distributed in a non-localized fashion throughout the cytoplasm, with YFP-
230 A3G but not genome or Gag-CFP accumulating at PBs (Fig. 3D, 2 and 3 h time points
231 post-onset of viral MS2-RFP gene expression). To begin to test if genomes and YFP-A3G
232 were interacting in the cytosolic fluid, we performed fluorescence recovery after
233 photobleaching (FRAP) analysis to measure rates of YFP-A3G recovery with or without
234 genomes and in the presence or absence of Gag (Fig. 3H, and quantification in Fig. 3I);
235 according to the hypothesis that interactions with bulky genomes would slow YFP-A3G
236 movements in the cytoplasm. To establish a baseline, we first infected cells with a Vif-
237 deficient HIV-1 reporter virus (Vifxx HIV mCherry), and confirmed that infection indeed
238 markedly reduced rates of YFP-A3G recovery ($t_{1/2}$ = 34.4 s +/- 5.3 s; *n*=8 cells) relative to
239 the uninfected (YFP-A3G alone) control ($t_{1/2}$ = 27.0 s +/- 13.5 s; *n*=14 cells). Interestingly,
240 we also observed incomplete recovery of YFP-A3G in infected cells (~75% recovery
241 compared to nearly 90% for untreated control cells Fig. 3I); consistent with the notion that
242 infection actually immobilized a significant fraction of the YFP-A3G pool within the
243 cytoplasm (74). To next dissect the relative contributions of genomes vs. Gag, we
244 compared YFP-A3G recovery after expressing genomes alone (Gagx/Vifxx visible HIV;
245 "Genome Only") to a "Gag Only" condition wherein we expressed mCherry-tagged Gag
246 from an mRNA modified to lack 5' and 3' viral regulatory RNA sequences and codon-
247 optimized to further reduce the potential for contributions of viral *cis*-acting RNA elements
248 located in the *gag* open reading frame (see cartoon depiction in Fig. 3G). The "Genome
249 Only" condition yielded markedly slower YFP-A3G recovery ($t_{1/2}$ = 70.8 s +/- 27.6 s; *n*=6
250 cells) relative to the no virus control (YFP-A3G Alone) and (COGag-mCh; $t_{1/2}$ = 30 s +/-

251 8.9 s; *n*=7 cells) (Fig. 3I). Combined, because expression of genomes but not Gag slowed
252 YFP-A3G movements in the cytoplasm based on FRAP analysis, we postulated that
253 genome-YFP-A3G interactions are initiated in the cytoplasm independently of Gag
254 expression and well prior to the onset of virus particle assembly.

255

256 **RNA tethering confirms genome-A3G interactions to be selective, Gag-**
257 **independent, and initiated soon after RNA nuclear export.**

258 Because FRAP does not distinguish between direct or indirect genome-A3G interactions,
259 we endeavored to develop a single cell assay based on RNA tethering that would allow
260 us to make more direct measurements of RNA-RBP interactions in the cytoplasm; dubbed
261 the In-Cell RNA-Protein Interaction Protocol (IC-IP) (depicted in Fig. 4A). The IC-IP was
262 based on the principle that, should RNA-protein interactions be sufficiently strong and
263 selective, tethering an RNA of interest to unnatural sites in the cytoplasm (*e.g.*,
264 membranes or the actin cytoskeleton) will shift the subcellular localization of the RBPs
265 that are strongly and persistently associated with that RNA.

266 For genome-A3G IC-IPs, MSL-bearing genomes served as "bait" for YFP-A3G
267 "prey", as depicted in Fig. 4A. Genome retargeting was achieved by co-expressing
268 "targeter" MS2 coat proteins modified to tether MSL-tagged genomes to either
269 membranes (Src-MS2; MS2 bearing an N-terminal 10 amino-acid membrane targeting
270 signal) or the actin cytoskeleton (Lifeact-MS2; bearing an N-terminal 17 amino acid F-
271 actin targeting signal) (Fig. 4B). Src-MS2 and Lifeact-MS2 targeters were expressed
272 fused to iRFP670 so that we could co-visualize the targeter with visible 2-color HIV-1
273 expressing Gag-CFP and genomes labelled with the self-tagging MS2-RFP "tracker" (see
274 cartoon depiction in Fig. 4C).

275 Co-expression of visible Vifxx Gag-CFP/MS2-RFP genomes as bait with the Src-
276 MS2-iRFP or Lifeact-MS2-iRFP targeters caused moderate re-localization of Gag-CFP
277 proteins from the cytosolic pool to intracellular vesicles (Fig. 4D, compare panels iv. and
278 ix.) or F-actin filaments (Fig. 4D, compare panels iv. to xiv.), respectively; consistent with

279 a subset of Gag proteins co-trafficking with their genome substrate in the cytosol as we
280 have previously shown (39). Effects on YFP-A3G, however, were more striking, with
281 >50% of the net YFP-A3G per cell fluorescent signal relocalized to intracellular vesicles
282 or F-actin filaments (Fig. 4D, compare panels ii., viii., and xiii., and see YFP-A3G regions-
283 of-interest; ROI; with quantification in Figs. 4E and 4F). Consistent with our FRAP
284 analyses (Figs. 3H and 3I), "Genome Only" bait was sufficient to recruit >50% of YFP-
285 A3G to intracellular vesicles as directed by Src-MS2, indicating that genome-A3G
286 cytosolic interactions are widespread and occur independently of Gag (Figs. 5A and 5B).
287 By contrast, tethering a control mRNA expressing codon-optimized version of CFP-
288 tagged Gag ("Gag Only") had no effect on YFP-A3G cytoplasmic distribution (Figs. 5C
289 and 5D), confirming specificity. Collectively, these results suggested that HIV-1 genome-
290 A3G interactions in the cytoplasm are strong, specific, and occur in the absence of Gag.

291 A useful feature of the IC-IP is that it can be carried out in live cells and coupled to
292 video microscopy to determine the timing of genome-RBP interactions relative to the
293 onset of RNA nuclear export. Live cell imaging of cells co-expressing Src-MS2-iRFP670
294 with a "Genome Only" RNA bait demonstrated YFP-A3G almost fully re-localized to
295 vesicles within two hours of the onset of viral gene expression and observations of
296 genomes exiting the nucleus (Fig. 5E, compare 1h and 2h time points, and see Movie S7
297 for detail). Accordingly, strong genome-A3G interactions are initiated concomitantly with
298 or very soon after genome nuclear export, and these interactions do not require Gag
299 expression.

300 To further address specificity, we performed similar experiments using Src- or
301 Lifeact-tethered genomes as bait for a variety of alternative co-expressed YFP-tagged

302 RBP preys including YFP-MOV10 and YFP-UPF1 (Figs. 5F and 5G and see Fig. S2 for
303 a compilation of representative images). Of this panel, only YFP-MOV10 exhibited a
304 particularly marked re-localization equivalent to if not more pronounced than YFP-A3G.
305 YFP-UPF1 localization was shifted by genome, but to a lesser extent (Figs. 5F and 5G).
306

307 **Tethering A3G to membranes arrests HIV-1 genome trafficking and inhibits virus**
308 **particle production.**

309 We reasoned that if A3G's interactions with genomes are sufficiently strong, then
310 tethering A3G to membranes would, as a corollary, arrest HIV-1 genome mobility in the
311 cytosol and abolish genome trafficking to sites of virus particle assembly. To test this
312 concept, we carried out the "reciprocal" IC-IP experiment outlined in Fig. 6A, wherein
313 YFP- or CFP-tagged A3G was modified to bind membranes using the same N-terminal
314 Src-derived myristoylation signal used for Src-MS2-directed RNA tethering. These fusion
315 proteins were co-expressed with two-color Vif-deficient visible HIV-1 (Vifxx Gag-
316 CFP/MS2-RFP) (Fig. 6B) or "Genome Only" (Vifxx Gagx/MS2-RFP) genomes (Fig. 6C).
317 As would be anticipated for a strong interaction, Src-FP-A3G expression induced marked
318 clustering of MS2-RFP-tagged genomes to perinuclear vesicles with (Fig. 6B) or without
319 (Fig. 6C) Gag expression, with genomes co-localizing with Src-FP-A3G in both instances.
320 To address the more relevant scenario of natively infected cells, we generated a stable
321 cell line constitutively expressing Src-YFP-A3G (HeLa.Src-YFP-A3G cells) and infected
322 these cells with Vifxx reporter virus (Fig. 6D). As expected, we genomes (and, to a lesser
323 extent, Gag) co-accumulated with Src-YFP-A3G at cytoplasmic vesicles at 24 hpi,
324 detected using combined IF/FISH (Fig. 6D, bottom, white arrows). Co-expression of Src-
325 YFP-A3G or a Src-MS2 control with MSL-tagged 2-color genome (Gag-BFP in this
326 experiment) yielded dose-dependent reduction to cytosolic Gag level and net efficiency
327 of virus particle release (Fig. 6E). Taken together, these experiments demonstrate that
328 A3G-genome interactions in the cytosol are sufficiently strong so that altering A3G

329 trafficking effectively repurposes this antiviral factor as a physical inhibitor of HIV-1
330 genome trafficking.
331
332

333 **A3G-genome interactions promote more consistent per virion delivery of A3G to**
334 **sites of virus particle assembly.**

335 Combined, the above experiments suggested that A3G preferentially recognizes one or
336 more HIV-1 genome RNA signatures even in the absence of Gag. However, a remaining
337 conundrum was that A3G is known to be encapsidated by Gag into virus particles even
338 in the absence of packageable genomes (23–25). In an effort to better rationalize prior
339 observations of A3G genome specificity vs. promiscuity, we performed comparative
340 single virion analysis (SVA) of A3G delivery into virus particles using a technique
341 pioneered by the Hu and Pathak groups wherein fluorescently-labeled virus-like particles
342 (VLPs) are harvested from HEK293T cells (that produce a greater quantity of particles
343 relative to HeLa) and subjected to sub-micron quantitative multicolor fluorescence
344 imaging to measure relative levels of per particle genome and/or A3G incorporation (42,
345 75) (Fig. 7). For this analysis, we compared per particle levels of YFP-A3G for four
346 independent Gag/genome scenarios (depicted in Fig. 7A); (1) "Gag-Only" mRNAs
347 encoding codon-optimized Gag-CFP (COGag-CFP = "Gag-Only"), viral (2) Vif+ or (3)
348 Vifxx 2-color HIV Gag-CFP/MS2-RFP genomes, or (4) mRNAs encoding codon-optimized
349 Gag-CFP wherein the NC RNA-binding domain was replaced by a leucine zipper
350 (ΔNCzip) to abolish Gag-RNA binding (based on (75, 76)). As expected, YFP-A3G
351 packaging was only observed for the COGag and the Vifxx HIV-1 conditions (Fig. 7B).

352 Using SVA, Vif+ and Vifxx viruses exhibited high efficiency MS2-RFP incorporation
353 (~89 and ~88% of Gag-CFP particles scoring positive for MS2-RFP, respectively),
354 consistent with a prior report of HIV-1 genome packaging efficiency (77). Vifxx Gag-
355 CFP/MS2-RFP particles exhibited a similar frequency of YFP-A3G incorporation (86% of

356 total Gag-CFP particles) (Fig. 7C and quantification in 7D). However, for “Gag-Only”
357 (COGag-CFP) particles, the frequency of detectable YFP-A3G incorporation was lower
358 (57% efficiency), intermediate to Vifxx HIV-1 vs. the ΔNCzip “no-RNA” negative control
359 (Fig. 7C and quantification in 7D). COGag particles also exhibited reduced per virion
360 levels of YFP-A3G fluorescence when compared to full-length, Vifxx HIV (Fig. 7C and
361 quantification in 7E). In sum, these data indicated that, although genomes are not
362 essential for YFP-A3G delivery to virus particles, selective genome-A3G interactions
363 promote a more consistent and more enriched per virion delivery of A3G to virus particle
364 assembly sites.

365 **DISCUSSION**

366 Herein we studied HIV-1 replication from the host cell perspective, using RBP biosensor
367 cell lines, visible HIV-1 viruses, and single-cell RNA-protein interaction assays. On a
368 technical level, our long-term imaging demonstrates that tagged RBP biosensors can be
369 used to detect and measure multivariate aspects of HIV-1 infection. For example, YFP-
370 A3G allows for measurements of Vif-mediated A3G degradation (Fig. 1D and Movie S1),
371 with movies demonstrating Vif's capacity to degrade A3G is potent, occurs ubiquitously
372 throughout the cell, and is remarkably persistent; lasting hours to days with little to no
373 evidence of fluctuations to Vif activity prior to induction of cell cycle arrest (Figs. 1D, E
374 and Movie S1). We also confirmed that NL4-3 Vif completes its degradation of A3G prior
375 to the onset of virion assembly (Fig. 3B), a result consistent with compelling recent work
376 from Holmes *et al*. who used a similar imaging-based approach to show that Gag's
377 trafficking to the plasma membrane is delayed until Vif has sufficient time to inactivate
378 A3G (78). Not all Vif alleles degrade A3G (79) or induce cell cycle arrest (80–82). Thus,
379 the A3G biosensor is emerging as a useful tool for categorizing single-cell Vif activities
380 found in circulating HIV strains and subtypes (83).

381 In the absence of Vif, HeLa.YFP-A3G cells were also able to detect virus particle
382 assembly (Figs. 1F, 1G, S1 and Movies S2, S3), a feat that could also be accomplished
383 using YFP-MOV10 even in the presence of Vif expression (Figs. 1I, S1, and Movie S3).
384 While it was not unexpected that A3G and/or MOV10 would be detected at sites of virus
385 particle assembly, based on prior studies (13, 75, 84), we were surprised to observe such
386 a massive re-distribution of YFP-A3G and YFP-MOV10 into large (assumed to be >2μm
387 diameter at current resolution) clusters of virus particles that remained associated with

388 the cell surface for hours to days, and could be transferred to neighboring cells (see
389 Movies S2 and S3). This clustering phenotype could be attributable, at least in part, to the
390 effects of BST2/Tetherin; a host restriction factor expressed constitutively in HeLa cells
391 that tethers enveloped virus particles to plasma membrane during and after budding (85,
392 86). However, our viruses encode an intact NL4-3 *vpu* gene that should antagonize
393 BST2/Tetherin. Alternatively, clustering may reflect interactions with charged surface
394 factors such as glycosaminoglycans, that we have previously shown to cause retroviral
395 particle co-clustering and cell retention ("surfacing") after budding; driven by electrostatic
396 interactions (87). Regardless, to our knowledge this is the first demonstration that HIV-1
397 assembly and transmission dynamics can be easily recorded using a proxy biosensor
398 (*i.e.*, without having to modify native viruses).

399 Despite HIV-1's marked effects on YFP-A3G and YFP-MOV10, we observed no
400 discernible effects of infection on canonical markers of SGs or PBs monitored using our
401 YFP-TIA-1 or CFP-DCP1A biosensors, respectively; with or without Vif expression (Fig.
402 2). We also observed no major changes to the distribution of NMD factor UPF1 (Fig. 1I,
403 Fig. S1, and Movie S3). These results confirm that HIV-1's effects on A3G and MOV10
404 subcellular trafficking are specific; and reinforce that HIV-1 does not modulate visible PBs
405 or induce the formation of SGs, even transiently. The underlying significance of A3G and
406 MOV10's localization to PBs and SGs remains unknown, but doing so positions these
407 proteins proximal to cytoplasmic mRNA surveillance machines that mediate miRNA-
408 dependent mRNA decay (PBs) or mRNA "triage" during stress responses (SGs) (33–35).
409 In theory, all successful viruses are adapted to subvert, suppress, or avoid such
410 responses; and HIV-1 (88, 89), other retroviruses (90, 91), and endogenous

411 retroelements including LINEs (92) and yeast Ty elements (93) hijack discrete
412 cytoplasmic RNP complexes as a means to compartmentalize key activities including
413 mRNA translation and genome packaging. Regarding suppression, Mouland and
414 colleagues have shown that HIV-1 and other retroviruses actively inhibit SG formation to
415 reduce the potential for cell stress initiated by promiscuous Gag NC binding to host RNAs
416 (69–71). Although we did not observe overt suppression of sodium arsenite-induced SGs
417 by HIV-1 in this study (Fig. 2G-I), the dynamics of these processes over the course of
418 infection warrant further investigation, and it is reasonable to posit that retroviruses must
419 avoid SGs to promote the fluid flow of genomes to capsid assembly sites. Overall,
420 however, our results are most consistent with a model wherein HIV-1's general *modus*
421 *operandi* is avoidance of PBs and SGs; with the key interactions underpinning host
422 protein packaging occurring ubiquitously throughout the cytosolic fluid.

423 Our FRAP and IC-IP results also demonstrate that HIV-1 genomes affect A3G
424 movements in the cytoplasm whether or not Gag capsid proteins are being expressed
425 (Figs. 3-6). Moreover, our data indicate that, in the context of natural infection, A3G (and
426 other RBPs such as MOV10) compete effectively with Gag for genome binding. For
427 example, more than 50% of cytosolic YFP-A3G and MOV-10 were recruited to
428 membranes or F-actin by Src- or Lifeact-MS2-tethered genomes, respectively (Fig. 4F);
429 effects less evident for Gag-CFP, not observed in the absence of genomes (Figs. 5D and
430 5G), and detected soon if not immediately after genome nuclear export (Fig. 5E). As to
431 *why* A3G-genome binding is selective, single virion analyses (Fig. 7) demonstrated an
432 ~90% frequency of A3G incorporation into genome-containing virions relative to "Gag-
433 only" particles, wherein the frequency of A3G incorporation was less than 60%. Taken

434 together, these results suggest that A3G combines both promiscuous (25) and targeted
435 (26) RNA binding mechanisms to ensure efficient packaging into HIV-1 virions, with the
436 targeted component enhancing per virion delivery and likely thereby maximizing A3G's
437 antiviral potential. Regarding the RNA signature detected by A3G, a prior study from York
438 et al. suggested a preference for A3G's binding to G-rich genome sequences (26), and
439 recent advances in viral epitranscriptomics shows that HIV-1 genomes are enriched
440 relative to host mRNAs in post-transcriptional regulatory marks including N^6
441 methyladenosine (m6a) (94–96); and also 5-methylcytosine (m5c) and 2'O-methylation
442 (97). The live cell tools described herein, in particular the IC-IP, should be useful for
443 further dissecting the extent of these interactions as they are occurring in cells.

444 In sum, our study confirms that the core, essential nature of viral RNA genome
445 trafficking in the cytosol occurs by diffusion in dynamic association with RNP complexes
446 that are smaller than PBs, with some proteins (*e.g.*, A3G and MOV10) more strongly
447 and/or more numerously associated with HIV-1 genomes than others. Because artificially
448 tethering A3G to membranes restricts HIV-1 genome trafficking and virus particle
449 production (Fig. 6), it also remains a possibility that these selective genome binding
450 features could ultimately be exploited in the context of an antiviral strategy.

451

452 **MATERIAL AND METHODS**

453 **Cell culture, plasmids, and stable cell lines.** Human HeLa and HEK293T cell lines
454 (obtained from ATCC) were cultured in DMEM (Sigma-Aldrich) supplemented with 10%
455 fetal bovine serum (heat-inactivated, filter-sterilized), 1% L-glutamine, and 1% penicillin-
456 streptomycin. HeLa.YFP-A3G, HEK293T.YFP-A3G, HeLa.Src-YFP-A3G, HeLa.YFP-
457 TIA-1, HeLa.CFP-DCP1A, HeLa-YFP-MOV10, and HeLa.YFP-UPF1 cell lines were
458 generated as previously described (39, 43). Briefly, relevant cDNAs were inserted into a
459 MIGR1-derived retroviral vector (pCMS28) (8) upstream of sequence encoding an
460 internal ribosome entry site (IRES) and a second reading frame encoding Puromycin-N-
461 acetyltransferase. Cells were selected by limiting dilution in the presence of 2μg/mL
462 puromycin. YFP, YFP-A3G, and Src-YFP-A3G as well as CFP versions of construct were
463 also generated using the pcDNA3.1 transient expression vector backbone (Invitrogen).
464 RBP expression constructs were cloned similarly into pCMS28, pcDNA3.1, or the
465 pSYFP2-C1 plasmid vector (a gift from Dorus Gadella, Addgene plasmid #22878;
466 http://n2t.net/addgene:22878; RRID:Addgene_22878) using cDNAs generated directly
467 from HeLa cell mRNA (RPL9, or RPS6, CBP80) or derived from the following sources:
468 DCP1A, TIA-1, and PABPC1 (28, 33, 44), MOV10 (a gift of Thomas Tuschl, Addgene
469 plasmid #10977) (45), UPF1 (a gift of Hal Dietz, Addgene plasmid #17708) (46), DDX3x
470 (47), and CRM1/XPO1 (48).

471 HIV-1 reporter virus plasmids were derived from a modified version of the pNL4-3
472 X4-tropic HIV-1 molecular clone (49) bearing inactivating mutations in *env*, *vpr*, and
473 expressing a green fluorescent protein (GFP) reporter from the *nef* locus (E-R-/GFP) (50);
474 with the GFP reporter replaced with either cerulean fluorescent protein (CFP) or mCherry

475 (mCh). Vif-minus HIV-1 reporter virus plasmids (Vifxx CFP and Vifxx mCherry) were
476 generated by changing *vif* codons 26 and 27 to stop codons informed by refs. (51, 52).
477 Two-color visible HIV-1 reporter viruses (Gag-CFP/MS2-RFP) were generated by
478 replacing the *gag* reading frame in Vif+ and Vifxx reporter viruses with *gag-CFP* just
479 upstream of sequence encoding 24 copies of the MS2 bacteriophage RNA stem loop
480 (MSL) (53), and inserting sequence encoding the MS2 coat protein fused to a red
481 fluorescence protein (RFP, either mApple or mCherry) and bearing an SV40 nuclear
482 localization signal (MS2-RFP). Gag was alternatively fused to mTagBFP2 for select
483 experiments (*e.g.*, Fig. 6E) in order to avoid cross-detection when immunoblotting for Src-
484 YFP-A3G using anti-GFP/YFP antisera. In all cases, mutated versions of full-length HIV-
485 1 were generated using overlapping PCR as previously described (39). Src-MS2-CFP,
486 Src-MS2-RFP, and Src-MS2-iRFP targeting constructs encoding an amino-terminal
487 membrane targeting signal derived from the Src kinase (MGSSKSKPKD) were generated
488 by overlapping PCR and subcloned into pcDNA3.1. mTagBFP2, mTurquoise2 (CFP), and
489 mApple (RFP) were gifts of Michael Davidson (Addgene plasmids # 54843, 54747, and
490 55302, respectively) (54, 55). iRFP670 cDNA (56) was amplified from the ColorfulCell
491 expression plasmid, a gift of Pierre Neveu (Addgene plasmid # 62449) (57).

492

493 **Retroviral assembly and infectivity assays**. Cells at 30-40% confluency were
494 transfected with 2µg DNA in six well plates using polyethylenimine (PEI; #23966,
495 Polysciences Inc.). pcDNA3.1 or pBlueScript were used as empty vector controls. Culture
496 media were replaced at 24 hours post-transfection and cell lysates and supernatants were
497 harvested for immunoblot analysis at 48 hours as previously described (58). Briefly, 1mL

498 of harvested culture supernatant was filtered, overlaid on 20% sucrose (w/v) in PBS,
499 subjected to centrifugation at >21,000g for two hours at 4ºC, and viral pellets were
500 resuspended in 35μL dissociation buffer (62.5 mM Tris-HCl, pH 6.8, 10% glycerol, 2%
501 sodium dodecyl sulfate [SDS], 5% β-mercaptoethanol). Cells were harvested in 500μL
502 radioimmunoprecipitation assay (RIPA) lysis buffer (10 mM Tris-HCl, pH 7.5, 150 mM
503 NaCl, 1 mM EDTA, 0.1% SDS, 1% Triton X-100, 1% sodium deoxycholate), homogenized
504 by passage through a 26G needle, subjected to centrifugation at 1,500g for 20 minutes
505 at 4ºC, and liquid supernatant fraction was combined 1:1 with 2X dissociation buffer.
506 Proteins were resolved by sodium dodecyl sulfate-polyacrylamide gel electrophoresis
507 (SDS-PAGE) and transferred to 0.2 μm nitrocellulose membranes. Gag was detected
508 using a mouse monoclonal antibody recognizing HIV-1 capsid/p24 (183-H12-5C; 1:1000
509 dilution) from Dr. Bruce Chesebro and obtained from the NIH AIDS Research and
510 Reference Reagent Program (Bethesda, MD, USA) (59) and anti-mouse secondary
511 antibodies conjugated to an infrared fluorophore (IRDye680LT, 1:10000 dilution, Li-Cor
512 Biosciences) for quantitative immunoblotting. As loading controls, heat shock protein
513 90A/B (HSP90) was detected using a rabbit polyclonal antibody (H-114, 1:2500 dilution,
514 Santa Cruz Biotechnology, Santa Cruz, CA, USA) or glyceraldehyde 3-phosphate
515 dehydrogenase (GAPDH) was detected using a mouse monoclonal antibody (6C5,
516 1:2500 dilution, Santa Cruz Biotechnology) and anti-rabbit or anti-mouse secondary
517 secondary antibodies conjugated to an infrared fluorophore (IRDye800CW, 1:7500
518 dilution, Li-Cor Biosciences). YFP-containing proteins (*e.g.*, YFP-A3G) were detected
519 using a rabbit polyclonal antibody recognizing GFP (FL sc-8334, 1:1000 dilution, Santa
520 Cruz Biotechnology) and anti-rabbit secondary antibodies conjugated to an infrared

521 fluorophore (IRDye800CW). For infectivity assays, supernatants containing single-round
522 infectious HIV-1 virions (pseudo-typed with VSV-G) were filtered and then added to target
523 HeLa cells in the presence of 10µg/mL polybrene. Approximately 36 hours later, target
524 HeLa cells were scanned using a BioTek Cytation5 to detect reporter CFP (455nm/510nm
525 excitation/emission filter) expression following infection.

526

527 **Microscopy, immunofluorescence, and fluorescence in situ hybridization (FISH).**
528 Cells were plated in 24-well glass-bottom plates (Eppendorf) or 8-well microslides (IBIDI)
529 and transfected using PEI or infected with HIV-1 reporter viruses. Transfection mixes
530 contained 1µg (24-well) or 333ng (IBIDI) total plasmid DNA, respectively. Infections were
531 performed with VSV-G pseudo-typed HIV-1 reporter viruses produced in HEK293T cells
532 and titered on HeLa cells to determine MOI of 0.5-1, thereby ensuring that ~33-66% of
533 the cells would be infected per experiment. Fixed-cell experiments were performed on a
534 Nikon Ti-Eclipse inverted wide-field microscope (Nikon Corporation, Melville, NY, USA)
535 using a 100x Plan Apo oil objective (numerical aperture [NA], 1.45). Transfected cells
536 were fixed 24 – 32 hours post-transfection and infected cells were fixed 42 hours post-
537 infection using 4% paraformaldehyde. If treated with 250 µM sodium arsenite (Sigma-
538 Aldrich), drug or an equivalent volume of dimethyl sulfoxide were added to cell culture
539 wells at approximately one hour prior to fixation and returned to incubation at 37ºC. Live-
540 cell imaging experiments were also performed on a Nikon Ti-Eclipse inverted wide-field
541 microscope using a 20x Plan Apo objective lens (NA, 0.75) with images acquired every
542 60 minutes (except where otherwise indicated) over a time course of 16 to 90 hours.
543 Images were acquired using an ORCA-Flash4.0 CMOS camera (Hammatsu Photonics)

544 and the following excitation/emission filter sets (nanometer ranges): BFP (402/455), CFP
545 (430/470), YFP (510/535), mApple (555/605), mCherry (572/632), and iRFP (645/705).
546 All images were processed and analyzed using FIJI/ImageJ2 (60). For IC-IP
547 colocalization analysis, ~10 targeter single cell iRFP+/RFP+ channel ROIs were chosen
548 at random, used to build ~1 μM z-stack max intensity projections prior to comparing the
549 overlap of iRFP (targeter) and YFP (RBP) channels using the Coloc2 plugin in
550 FIJI/ImageJ2.

551 For fixed-cell experiments using FISH, cells were plated as described as above
552 and previously (39). At 42 hours post-infection or after 24 hours plated (for uninfected
553 cells), cells were washed, fixed in 4% formaldehyde, and permeabilized in 70% ethanol
554 for at least 4 hours at 4ºC. Custom Stellaris FISH probes were designed to recognize
555 NL4-3 HIV-1 *gag-pol* reading frame nucleotides 386-4456 using the Stellaris RNA FISH
556 Probe Designer 4.1 (Biosearch Technologies, Inc.) available online. To detect *yfp*
557 mRNAs, we used a DesignReady Probe set specific to eGFP. Both probe sets were
558 labeled with CAL Fluor Red 590 Dye (Biosearch Technologies, Inc.). Samples were
559 hybridized with the *gag/gag-pol* probe set according to the manufacturer's instructions
560 available online. Simultaneous immunofluorescence to detect Gag used a mouse
561 monoclonal antibody specific to p24 (#24-2, a gift of Dr. Michael Malim). Imaging
562 experiments were performed as described above on a Nikon Ti-Eclipse inverted wide-
563 field microscope using a 100x Plan Apo objective lens.

564 FRAP experiments were performed using a Nikon Ti-Eclipse inverted A1R+
565 resonant/galvano hybrid confocal line-scanning microscope. Images were captured using
566 a 20x Plan Apo objective lens (NA, 0.75) and GaAsP multi-detector for 488 and 560nm

567 channels. YFP-A3G was imaged using the 488nm laser at a low arbitrary intensity and
568 photobleached using the laser's maximum intensity. MS2-RFP and COGag-mCherry
569 were imaged using the 560nm laser at a low arbitrary intensity. Cells were maintained in
570 an environmental chamber (Pathology Devices, Inc.) at 37ºC, 5% CO_2, and 50% humidity.
571 Cells were imaged every 30 seconds for 4 frames prior to photobleaching (3 rapid
572 ablations of cytoplasmic ROIs 10μm in diameter) followed by imaging every 5 seconds
573 for a minute, every 15 seconds for four minutes, and every 30 seconds for 5 minutes. This
574 time frame was sufficient for fluorescence recovery to reach a plateau. FRAP analysis
575 was performed using the FIJI plugin FRAP Profiler (61) that adjusts for incidental field
576 photobleaching outside the ROI but within the cell of interest.

577 Single virion analyses (SVA) were performed largely as described by Chen *et al.*
578 (42). Virus particles were produced as described above for western blotting in
579 HEK293T.YFP-A3G cells to maintain consistent levels of YFP-A3G as compared to co-
580 transfection. Filtered culture supernatants (750μL) were purified by sucrose centrifugation
581 as described above and resuspended in 100μL 1x PBS (Sigma-Aldrich). 24-well plates
582 were pre-coated with 2% FBS diluted in 1x PBS for at least 30 minutes, this solution was
583 removed, and the resuspended concentrated virus particles were added to wells. Images
584 were acquired on a Nikon Ti-Eclipse inverted wide-field microscope using a 100x Plan
585 Apo objective lens (NA, 1.45). These images were processed and analyzed using
586 Analyze Particles plugin in FIJI/ImageJ2 (60).

587

588 **Thin-section electron microscopy.** HeLa.YFP-A3G were infected with Vif+ CFP or
589 Vifxx CFP HIV-1 viruses and fixed at 48 hours for chemical processing as previously

590 described (62). Samples were sectioned into 100nm slices and with sections collected on
591 copper thin-bar grids. Sections were observed with a Phillips CM120 transmission
592 electron microscope, and images were collected with a MegaView III (Olympus-SIS,
593 Lakewood, CO, USA) side-mounted digital camera. All images were processed and
594 analyzed using FIJI/ImageJ2 (60).

595

596 **Statistics.** For assembly assays (e.g., Figs. 1C and 6E), results were obtained from three
597 independent biological replicates; defined as cells plated and processed on different days.
598 Graphs plot the mean value with error bars representing the standard deviation of the
599 mean with the exception of Fig. 5G, that shows the second and third quartiles and Fig.
600 7E, a violin plot showing all data points with the mean (solid line) and quartiles (dashed
601 lines) indicated. All statistical comparisons were carried out using the two-tailed
602 Student's *t* test and performed using Microsoft Excel or Graphpad Prism.

603

604 **ACKNOWLEDGEMENTS**

605 This study was supported by National Institutes of Health [R01AI110221, U54AI150470
606 to N.M.S., T32CA009135 to E.L.E.III, and T32GM008349 to B.E.B.]; the Wisconsin
607 Partnership Program New Investigator Program [ID 2830 to N.M.S.]; the Greater
608 Milwaukee Foundation's Shaw Scientist Program [to N.M.S.]; a UW-Madison UW2020
609 Infrastructure Award [to N.M.S]; a UW—Madison office of the Vice Chancellor of
610 Research and Graduate Education (OVCGRE) Research Competition Award [to N.M.S.];
611 two National Science Foundation Graduate Research Fellowships [DGE-1256259 to
612 J.T.B. and B.E.B.], an OVCGRE Dissertation Completion Fellowship [to J.T.B.]; an
613 Advance Opportunity Fellowship from the UW-Madison SciMed/GRS program [to
614 E.L.E.III].; and a UW-Madison Hilldale Undergraduate Research Fellowship [to S.L.P.].
615 Any opinions, findings, and conclusions or recommendations expressed in this material
616 are those of the authors and do not necessarily reflect the views of the National Science
617 Foundation.

618 We thank Randall Massey at the University of Wisconsin SMPH Electron
619 Microscopy Facility for assistance with EM sample preparation. We are grateful to Michael
620 Malim (King's College London), Chad Swanson, (King's College London), and Sarah
621 Gallois-Montbrun (Institut Cochin) for plasmid reagents and advice. The following reagent
622 was obtained through the NIH AIDS Reagent Program, Division of AIDS, NIAID, NIH:
623 HIV-1 p24 hybridoma (183-H12-5C) (from Bruce Chesebro) (59). We thank Kelly Watters,
624 Marchel Hill, and Ann Palmenberg for RVA16.

625

626 **REFERENCES**

627 1. Bolinger C, Boris-Lawrie K. 2009. Mechanisms employed by retroviruses to exploit
628 host factors for translational control of a complicated proteome. Retrovirology 6:8.

629 2. Cochrane AW, McNally MT, Mouland AJ. 2006. The retrovirus RNA trafficking
630 granule: from birth to maturity. Retrovirology 3:18.

631 3. Karn J, Stoltzfus CM. 2012. Transcriptional and posttranscriptional regulation of HIV-
632 1 gene expression. Cold Spring Harb Perspect Med 2:a006916.

633 4. Swanson CM, Malim MH. 2006. Retrovirus RNA trafficking: from chromatin to
634 invasive genomes. Traffic 7:1440–1450.

635 5. Harris RS, Bishop KN, Sheehy AM, Craig HM, Petersen-Mahrt SK, Watt IN,
636 Neuberger MS, Malim MH. 2003. DNA deamination mediates innate immunity to
637 retroviral infection. Cell 113:803–809.

638 6. Malim MH. 2009. APOBEC proteins and intrinsic resistance to HIV-1 infection.
639 Philos Trans R Soc Lond, B, Biol Sci 364:675–687.

640 7. Refsland EW, Harris RS. 2013. The APOBEC3 family of retroelement restriction
641 factors. Curr Top Microbiol Immunol 371:1–27.

642 8. Sheehy AM, Gaddis NC, Choi JD, Malim MH. 2002. Isolation of a human gene that
643 inhibits HIV-1 infection and is suppressed by the viral Vif protein. Nature 418:646–
644 650.

645 9. Mariani R, Chen D, Schröfelbauer B, Navarro F, König R, Bollman B, Münk C,
646 Nymark-McMahon H, Landau NR. 2003. Species-specific exclusion of APOBEC3G
647 from HIV-1 virions by Vif. Cell 114:21–31.

648 10. Sheehy AM, Gaddis NC, Malim MH. 2003. The antiretroviral enzyme APOBEC3G
649 is degraded by the proteasome in response to HIV-1 Vif. Nat Med 9:1404–1407.

650 11. Stopak K, de Noronha C, Yonemoto W, Greene WC. 2003. HIV-1 Vif blocks the
651 antiviral activity of APOBEC3G by impairing both its translation and intracellular
652 stability. Mol Cell 12:591–601.

653 12. Serquiña AKP, Das SR, Popova E, Ojelabi OA, Roy CK, Göttlinger HG. 2013.
654 UPF1 is crucial for the infectivity of human immunodeficiency virus type 1 progeny
655 virions. J Virol 87:8853–8861.

656 13. Burdick R, Smith JL, Chaipan C, Friew Y, Chen J, Venkatachari NJ, Delviks-
657 Frankenberry KA, Hu W-S, Pathak VK. 2010. P body-associated protein Mov10
658 inhibits HIV-1 replication at multiple stages. J Virol 84:10241–10253.

659 14. Wang X, Han Y, Dang Y, Fu W, Zhou T, Ptak RG, Zheng Y-H. 2010. Moloney
660 leukemia virus 10 (MOV10) protein inhibits retrovirus replication. J Biol Chem
661 285:14346–14355.

662 15. Ajamian L, Abrahamyan L, Milev M, Ivanov PV, Kulozik AE, Gehring NH, Mouland
663 AJ. 2008. Unexpected roles for UPF1 in HIV-1 RNA metabolism and translation.
664 RNA 14:914–927.

665 16. Knoener RA, Becker JT, Scalf M, Sherer NM, Smith LM. 2017. Elucidating the in
666 vivo interactome of HIV-1 RNA by hybridization capture and mass spectrometry.
667 Sci Rep 7:16965.

668 17. Freed EO. 2015. HIV-1 assembly, release and maturation. Nat Rev Microbiol
669 13:484–496.

670 18. Sundquist WI, Kräusslich H-G. 2012. HIV-1 assembly, budding, and maturation.
671 Cold Spring Harb Perspect Med 2:a006924.

672 19. Eckwahl MJ, Arnion H, Kharytonchyk S, Zang T, Bieniasz PD, Telesnitsky A, Wolin
673 SL. 2016. Analysis of the human immunodeficiency virus-1 RNA packageome.
674 RNA 22:1228–1238.

675 20. Rulli SJ, Hibbert CS, Mirro J, Pederson T, Biswal S, Rein A. 2007. Selective and
676 nonselective packaging of cellular RNAs in retrovirus particles. J Virol 81:6623–
677 6631.

678 21. Zennou V, Perez-Caballero D, Göttlinger H, Bieniasz PD. 2004. APOBEC3G
679 incorporation into human immunodeficiency virus type 1 particles. J Virol
680 78:12058–12061.

681 22. Khan MA, Goila-Gaur R, Opi S, Miyagi E, Takeuchi H, Kao S, Strebel K. 2007.
682 Analysis of the contribution of cellular and viral RNA to the packaging of
683 APOBEC3G into HIV-1 virions. Retrovirology 4:48.

684 23. Cen S, Guo F, Niu M, Saadatmand J, Deflassieux J, Kleiman L. 2004. The
685 interaction between HIV-1 Gag and APOBEC3G. J Biol Chem 279:33177–33184.

686 24. Alce TM, Popik W. 2004. APOBEC3G is incorporated into virus-like particles by a
687 direct interaction with HIV-1 Gag nucleocapsid protein. J Biol Chem 279:34083–
688 34086.

689 25. Apolonia L, Schulz R, Curk T, Rocha P, Swanson CM, Schaller T, Ule J, Malim
690 MH. 2015. Promiscuous RNA binding ensures effective encapsidation of
691 APOBEC3 proteins by HIV-1. PLoS Pathog 11:e1004609.

692 26. York A, Kutluay SB, Errando M, Bieniasz PD. 2016. The RNA Binding Specificity of
693 Human APOBEC3 Proteins Resembles That of HIV-1 Nucleocapsid. PLoS Pathog
694 12:e1005833.

695 27. Svarovskaia ES, Xu H, Mbisa JL, Barr R, Gorelick RJ, Ono A, Freed EO, Hu W-S,
696 Pathak VK. 2004. Human apolipoprotein B mRNA-editing enzyme-catalytic
697 polypeptide-like 3G (APOBEC3G) is incorporated into HIV-1 virions through
698 interactions with viral and nonviral RNAs. J Biol Chem 279:35822–35828.

699 28. Gallois-Montbrun S, Holmes RK, Swanson CM, Fernández-Ocaña M, Byers HL,
700 Ward MA, Malim MH. 2008. Comparison of cellular ribonucleoprotein complexes
701 associated with the APOBEC3F and APOBEC3G antiviral proteins. J Virol
702 82:5636–5642.

703 29. Maeda K, Almofty SA, Singh SK, Eid MMA, Shimoda M, Ikeda T, Koito A, Pham P,
704 Goodman MF, Sakaguchi N. 2013. GANP interacts with APOBEC3G and facilitates

705 its encapsidation into the virions to reduce HIV-1 infectivity. J Immunol 191:6030–
706 6039.

707 30. Zhen A, Du J, Zhou X, Xiong Y, Yu X-F. 2012. Reduced APOBEC3H variant anti-
708 viral activities are associated with altered RNA binding activities. PLoS ONE
709 7:e38771.

710 31. Bach D, Peddi S, Mangeat B, Lakkaraju A, Strub K, Trono D. 2008.
711 Characterization of APOBEC3G binding to 7SL RNA. Retrovirology 5:54.

712 32. Wang T, Tian C, Zhang W, Luo K, Sarkis PTN, Yu L, Liu B, Yu Y, Yu X-F. 2007.
713 7SL RNA mediates virion packaging of the antiviral cytidine deaminase
714 APOBEC3G. J Virol 81:13112–13124.

715 33. Gallois-Montbrun S, Kramer B, Swanson CM, Byers H, Lynham S, Ward M, Malim
716 MH. 2007. Antiviral protein APOBEC3G localizes to ribonucleoprotein complexes
717 found in P bodies and stress granules. J Virol 81:2165–2178.

718 34. Wichroski MJ, Robb GB, Rana TM. 2006. Human retroviral host restriction factors
719 APOBEC3G and APOBEC3F localize to mRNA processing bodies. PLoS Pathog
720 2:e41.

721 35. Nathans R, Chu C-Y, Serquina AK, Lu C-C, Cao H, Rana TM. 2009. Cellular
722 microRNA and P bodies modulate host-HIV-1 interactions. Mol Cell 34:696–709.

723 36. Chable-Bessia C, Meziane O, Latreille D, Triboulet R, Zamborlini A, Wagschal A,
724 Jacquet J-M, Reynes J, Levy Y, Saib A, Bennasser Y, Benkirane M. 2009.
725 Suppression of HIV-1 replication by microRNA effectors. Retrovirology 6:26.

726 37. Phalora PK, Sherer NM, Wolinsky SM, Swanson CM, Malim MH. 2012. HIV-1
727 replication and APOBEC3 antiviral activity are not regulated by P bodies. J Virol
728 86:11712–11724.

729 38. Pocock GM, Becker JT, Swanson CM, Ahlquist P, Sherer NM. 2016. HIV-1 and M-
730 PMV RNA Nuclear Export Elements Program Viral Genomes for Distinct
731 Cytoplasmic Trafficking Behaviors. PLoS Pathog 12:e1005565.

732 39. Becker JT, Sherer NM. 2017. Subcellular Localization of HIV-1 gag-pol mRNAs
733 Regulates Sites of Virion Assembly. J Virol 91.

734 40. Izumi T, Burdick R, Shigemi M, Plisov S, Hu W-S, Pathak VK. 2013. Mov10 and
735 APOBEC3G localization to processing bodies is not required for virion
736 incorporation and antiviral activity. J Virol 87:11047–11062.

737 41. Jouvenet N, Simon SM, Bieniasz PD. 2009. Imaging the interaction of HIV-1
738 genomes and Gag during assembly of individual viral particles. Proc Natl Acad Sci
739 USA 106:19114–19119.

740 42. Chen J, Grunwald D, Sardo L, Galli A, Plisov S, Nikolaitchik OA, Chen D, Lockett
741 S, Larson DR, Pathak VK, Hu W-S. 2014. Cytoplasmic HIV-1 RNA is mainly
742 transported by diffusion in the presence or absence of Gag protein. Proc Natl Acad
743 Sci USA 111:E5205-5213.

744 43. Sherer NM, Lehmann MJ, Jimenez-Soto LF, Ingmundson A, Horner SM, Cicchetti
745 G, Allen PG, Pypaert M, Cunningham JM, Mothes W. 2003. Visualization of
746 retroviral replication in living cells reveals budding into multivesicular bodies. Traffic
747 4:785–801.

748 44. Kedersha NL, Gupta M, Li W, Miller I, Anderson P. 1999. RNA-binding proteins
749 TIA-1 and TIAR link the phosphorylation of eIF-2 alpha to the assembly of
750 mammalian stress granules. J Cell Biol 147:1431–1442.

751 45. Meister G, Landthaler M, Peters L, Chen PY, Urlaub H, Lührmann R, Tuschl T.
752 2005. Identification of novel argonaute-associated proteins. Curr Biol 15:2149–
753 2155.

754 46. Mendell JT, ap Rhys CMJ, Dietz HC. 2002. Separable roles for rent1/hUpf1 in
755 altered splicing and decay of nonsense transcripts. Science 298:419–422.

756 47. Yedavalli VSRK, Neuveut C, Chi Y-H, Kleiman L, Jeang K-T. 2004. Requirement of
757 DDX3 DEAD box RNA helicase for HIV-1 Rev-RRE export function. Cell 119:381–
758 392.

759 48. Behrens RT, Aligeti M, Pocock GM, Higgins CA, Sherer NM. 2017. Nuclear Export
760 Signal Masking Regulates HIV-1 Rev Trafficking and Viral RNA Nuclear Export. J
761 Virol 91.

762 49. Adachi A, Gendelman HE, Koenig S, Folks T, Willey R, Rabson A, Martin MA.
763 1986. Production of acquired immunodeficiency syndrome-associated retrovirus in

764 human and nonhuman cells transfected with an infectious molecular clone. J Virol
765 59:284–291.

766 50. Connor RI, Chen BK, Choe S, Landau NR. 1995. Vpr is required for efficient
767 replication of human immunodeficiency virus type-1 in mononuclear phagocytes.
768 Virology 206:935–944.

769 51. Simon JH, Miller DL, Fouchier RA, Soares MA, Peden KW, Malim MH. 1998. The
770 regulation of primate immunodeficiency virus infectivity by Vif is cell species
771 restricted: a role for Vif in determining virus host range and cross-species
772 transmission. EMBO J 17:1259–1267.

773 52. Simon JH, Southerling TE, Peterson JC, Meyer BE, Malim MH. 1995.
774 Complementation of vif-defective human immunodeficiency virus type 1 by primate,
775 but not nonprimate, lentivirus vif genes. J Virol 69:4166–4172.

776 53. Femino AM, Fay FS, Fogarty K, Singer RH. 1998. Visualization of single RNA
777 transcripts in situ. Science 280:585–590.

778 54. Subach OM, Cranfill PJ, Davidson MW, Verkhusha VV. 2011. An enhanced
779 monomeric blue fluorescent protein with the high chemical stability of the
780 chromophore. PLoS ONE 6:e28674.

781 55. Goedhart J, von Stetten D, Noirclerc-Savoye M, Lelimousin M, Joosen L, Hink MA,
782 van Weeren L, Gadella TWJ, Royant A. 2012. Structure-guided evolution of cyan
783 fluorescent proteins towards a quantum yield of 93%. Nat Commun 3:751.

784 56. Shcherbakova DM, Verkhusha VV. 2013. Near-infrared fluorescent proteins for
785 multicolor in vivo imaging. Nat Methods 10:751–754.

786 57. Sladitschek HL, Neveu PA. 2015. MXS-Chaining: A Highly Efficient Cloning
787 Platform for Imaging and Flow Cytometry Approaches in Mammalian Systems.
788 PLoS ONE 10:e0124958.

789 58. Sherer NM, Swanson CM, Hué S, Roberts RG, Bergeron JRC, Malim MH. 2011.
790 Evolution of a species-specific determinant within human CRM1 that regulates the
791 post-transcriptional phases of HIV-1 replication. PLoS Pathog 7:e1002395.

792 59. Chesebro B, Wehrly K, Nishio J, Perryman S. 1992. Macrophage-tropic human
793 immunodeficiency virus isolates from different patients exhibit unusual V3 envelope
794 sequence homogeneity in comparison with T-cell-tropic isolates: definition of critical
795 amino acids involved in cell tropism. J Virol 66:6547–6554.

796 60. Schindelin J, Arganda-Carreras I, Frise E, Kaynig V, Longair M, Pietzsch T,
797 Preibisch S, Rueden C, Saalfeld S, Schmid B, Tinevez J-Y, White DJ, Hartenstein
798 V, Eliceiri K, Tomancak P, Cardona A. 2012. Fiji: an open-source platform for
799 biological-image analysis. Nat Methods 9:676–682.

800 61. Hardin J. 2011. Imaging embryonic morphogenesis in C. elegans. Methods Cell
801 Biol 106:377–412.

802 62. Garcia-Miranda P, Becker JT, Benner BE, Blume A, Sherer NM, Butcher SE. 2016.
803 Stability of HIV Frameshift Site RNA Correlates with Frameshift Efficiency and
804 Decreased Virus Infectivity. J Virol 90:6906–6917.

805 63. Ivanov P, Kedersha N, Anderson P. 2019. Stress Granules and Processing Bodies
806 in Translational Control. Cold Spring Harb Perspect Biol 11.

807 64. Kedersha N, Cho MR, Li W, Yacono PW, Chen S, Gilks N, Golan DE, Anderson P.
808 2000. Dynamic shuttling of TIA-1 accompanies the recruitment of mRNA to
809 mammalian stress granules. J Cell Biol 151:1257–1268.

810 65. Sakai K, Dimas J, Lenardo MJ. 2006. The Vif and Vpr accessory proteins
811 independently cause HIV-1-induced T cell cytopathicity and cell cycle arrest. Proc
812 Natl Acad Sci USA 103:3369–3374.

813 66. Evans EL, Becker JT, Fricke SL, Patel K, Sherer NM. 2018. HIV-1 Vif's Capacity
814 To Manipulate the Cell Cycle Is Species Specific. J Virol 92.

815 67. Rao S, Amorim R, Niu M, Temzi A, Mouland AJ. 2018. The RNA surveillance
816 proteins UPF1, UPF2 and SMG6 affect HIV-1 reactivation at a post-transcriptional
817 level. Retrovirology 15:42.

818 68. Watters K, Inankur B, Gardiner JC, Warrick J, Sherer NM, Yin J, Palmenberg AC.
819 2017. Differential Disruption of Nucleocytoplasmic Trafficking Pathways by
820 Rhinovirus 2A Proteases. J Virol 91.

821 69. Cinti A, Le Sage V, Ghanem M, Mouland AJ. 2016. HIV-1 Gag Blocks Selenite-
822 Induced Stress Granule Assembly by Altering the mRNA Cap-Binding Complex.
823 MBio 7:e00329.

824 70. Valiente-Echeverría F, Melnychuk L, Vyboh K, Ajamian L, Gallouzi IE, Bernard N,
825 Mouland AJ. 2014. eEF2 and Ras-GAP SH3 domain-binding protein (G3BP1)
826 modulate stress granule assembly during HIV-1 infection. Nat Commun 5:4819.

827 71. Monette A, Niu M, Chen L, Rao S, Gorelick RJ, Mouland AJ. 2020. Pan-retroviral
828 Nucleocapsid-Mediated Phase Separation Regulates Genomic RNA Positioning
829 and Trafficking. Cell Rep 31:107520.

830 72. Rao S, Hassine S, Monette A, Amorim R, DesGroseillers L, Mouland AJ. 2019.
831 HIV-1 requires Staufen1 to dissociate stress granules and to produce infectious
832 viral particles. RNA 25:727–736.

833 73. Protter DSW, Parker R. 2016. Principles and Properties of Stress Granules. Trends
834 Cell Biol 26:668–679.

835 74. Ishikawa-Ankerhold HC, Ankerhold R, Drummen GPC. 2012. Advanced
836 fluorescence microscopy techniques--FRAP, FLIP, FLAP, FRET and FLIM.
837 Molecules 17:4047–4132.

838 75. Desimmie BA, Burdick RC, Izumi T, Doi H, Shao W, Alvord WG, Sato K, Koyanagi
839 Y, Jones S, Wilson E, Hill S, Maldarelli F, Hu W-S, Pathak VK. 2016. APOBEC3
840 proteins can copackage and comutate HIV-1 genomes. Nucleic Acids Res
841 44:7848–7865.

842 76. Accola MA, Strack B, Göttlinger HG. 2000. Efficient particle production by minimal
843 Gag constructs which retain the carboxy-terminal domain of human

844 immunodeficiency virus type 1 capsid-p2 and a late assembly domain. J Virol
845 74:5395–5402.

846 77. Chen J, Nikolaitchik O, Singh J, Wright A, Bencsics CE, Coffin JM, Ni N, Lockett S,
847 Pathak VK, Hu W-S. 2009. High efficiency of HIV-1 genomic RNA packaging and
848 heterozygote formation revealed by single virion analysis. Proc Natl Acad Sci USA
849 106:13535–13540.

850 78. Holmes M, Zhang F, Bieniasz PD. 2015. Single-Cell and Single-Cycle Analysis of
851 HIV-1 Replication. PLoS Pathog 11:e1004961.

852 79. Binka M, Ooms M, Steward M, Simon V. 2012. The activity spectrum of Vif from
853 multiple HIV-1 subtypes against APOBEC3G, APOBEC3F, and APOBEC3H. J
854 Virol 86:49–59.

855 80. Salamango DJ, Ikeda T, Moghadasi SA, Wang J, McCann JL, Serebrenik AA,
856 Ebrahimi D, Jarvis MC, Brown WL, Harris RS. 2019. HIV-1 Vif Triggers Cell Cycle
857 Arrest by Degrading Cellular PPP2R5 Phospho-regulators. Cell Rep 29:1057-
858 1065.e4.

859 81. Greenwood EJ, Matheson NJ, Wals K, van den Boomen DJ, Antrobus R,
860 Williamson JC, Lehner PJ. 2016. Temporal proteomic analysis of HIV infection
861 reveals remodelling of the host phosphoproteome by lentiviral Vif variants. Elife 5.

862 82. Zhao K, Du J, Rui Y, Zheng W, Kang J, Hou J, Wang K, Zhang W, Simon VA, Yu
863 X-F. 2015. Evolutionarily conserved pressure for the existence of distinct G2/M cell
864 cycle arrest and A3H inactivation functions in HIV-1 Vif. Cell Cycle 14:838–847.

865 83. Wang J, Becker JT, Shi K, Lauer KV, Salamango DJ, Aihara H, Shaban NM, Harris
866 RS. 2019. The Role of RNA in HIV-1 Vif-Mediated Degradation of APOBEC3H. J
867 Mol Biol 431:5019–5031.

868 84. Burnett A, Spearman P. 2007. APOBEC3G multimers are recruited to the plasma
869 membrane for packaging into human immunodeficiency virus type 1 virus-like
870 particles in an RNA-dependent process requiring the NC basic linker. J Virol
871 81:5000–5013.

872 85. Neil SJD, Zang T, Bieniasz PD. 2008. Tetherin inhibits retrovirus release and is
873 antagonized by HIV-1 Vpu. Nature 451:425–430.

874 86. Van Damme N, Goff D, Katsura C, Jorgenson RL, Mitchell R, Johnson MC,
875 Stephens EB, Guatelli J. 2008. The interferon-induced protein BST-2 restricts HIV-
876 1 release and is downregulated from the cell surface by the viral Vpu protein. Cell
877 Host Microbe 3:245–252.

878 87. Sherer NM, Jin J, Mothes W. 2010. Directional spread of surface-associated
879 retroviruses regulated by differential virus-cell interactions. J Virol 84:3248–3258.

880 88. Reed JC, Molter B, Geary CD, McNevin J, McElrath J, Giri S, Klein KC, Lingappa
881 JR. 2012. HIV-1 Gag co-opts a cellular complex containing DDX6, a helicase that
882 facilitates capsid assembly. J Cell Biol 198:439–456.

883 89. Barajas BC, Tanaka M, Robinson BA, Phuong DJ, Chutiraka K, Reed JC, Lingappa
884 JR. 2018. Identifying the assembly intermediate in which Gag first associates with

885 unspliced HIV-1 RNA suggests a novel model for HIV-1 RNA packaging. PLoS
886 Pathog 14:e1006977.

887 90. Soto-Rifo R, Valiente-Echeverria F, Rubilar PS, Garcia-de-Gracia F, Ricci EP,
888 Limousin T, Décimo D, Mouland AJ, Ohlmann T. 2014. HIV-2 genomic RNA
889 accumulates in stress granules in the absence of active translation. Nucleic Acids
890 Res 42:12861–12875.

891 91. Bann DV, Beyer AR, Parent LJ. 2014. A murine retrovirus co-Opts YB-1, a
892 translational regulator and stress granule-associated protein, to facilitate virus
893 assembly. J Virol 88:4434–4450.

894 92. Goodier JL, Zhang L, Vetter MR, Kazazian HH. 2007. LINE-1 ORF1 protein
895 localizes in stress granules with other RNA-binding proteins, including components
896 of RNA interference RNA-induced silencing complex. Mol Cell Biol 27:6469–6483.

897 93. Larsen LSZ, Beliakova-Bethell N, Bilanchone V, Zhang M, Lamsa A, Dasilva R,
898 Hatfield GW, Nagashima K, Sandmeyer S. 2008. Ty3 nucleocapsid controls
899 localization of particle assembly. J Virol 82:2501–2514.

900 94. Kennedy EM, Bogerd HP, Kornepati AVR, Kang D, Ghoshal D, Marshall JB, Poling
901 BC, Tsai K, Gokhale NS, Horner SM, Cullen BR. 2016. Posttranscriptional m(6)A
902 Editing of HIV-1 mRNAs Enhances Viral Gene Expression. Cell Host Microbe
903 19:675–685.

904 95. Lichinchi G, Gao S, Saletore Y, Gonzalez GM, Bansal V, Wang Y, Mason CE,
905 Rana TM. 2016. Dynamics of the human and viral m(6)A RNA methylomes during
906 HIV-1 infection of T cells. Nat Microbiol 1:16011.

907 96. Tirumuru N, Zhao BS, Lu W, Lu Z, He C, Wu L. 2016. N(6)-methyladenosine of
908 HIV-1 RNA regulates viral infection and HIV-1 Gag protein expression. Elife 5.

909 97. Courtney DG, Tsai K, Bogerd HP, Kennedy EM, Law BA, Emery A, Swanstrom R,
910 Holley CL, Cullen BR. 2019. Epitranscriptomic Addition of m5C to HIV-1
911 Transcripts Regulates Viral Gene Expression. Cell Host Microbe 26:217-227.e6.

912

913 **FIGURE LEGENDS**

914 **Figure 1.** Tracking the HIV-1 replication cycle using a YFP-A3G biosensor cell line. (A**)**
915 HeLa.YFP-A3G cells showing diffuse and punctate (processing bodies, PB, white arrows)
916 distribution of YFP-A3G at steady-state (left) and accumulation into stress granules (SGs,
917 magenta arrows) following 250 μM arsenite treatment (right, Ars). **(B)** Schematic of Vif-
918 competent (Vif+) or Vif-deficient (Vifxx) HIV-1 NL4-3 Env-, Vpr-, CFP reporter virus
919 genome. **(C)** Single-round infection confirms YFP-A3G-mediated restriction of HIV-1 in
920 the absence of Vif. 293T.YFP-A3G cells were transfected to generate the indicated HIV-
921 1 reporter viruses with or without co-expression of Vif-mCherry. Cells and virus particles
922 (*n*=3) were harvested at 48 h post-transfection and analyzed by quantitative immunoblot
923 using anti-p24^{Gag}, anti-YFP, and anti-HSP90 (loading control) antisera. **(D)**
924 Representative images from long-term time-lapse imaging showing degradation of YFP-
925 A3G after HIV-1 Vif+ CFP infection and Vif-dependent G2/M arrest at later (~48h) time
926 points. Figure corresponds to Supplementary Movie 1. **(E)** Quantification of movies
927 (IntDen) represented in (D) (Vif+, solid lines) and (Vifxx, dashed lines). Cells from 3
928 independent experiments (*n*=33) with $\geq$16 hours per cell (1 image/hour). **(F)**
929 Representative images from long-term time-lapse imaging of YFP-A3G upon HIV-1 Vifxx
930 CFP infection. Magenta boxes highlight regions of interest (ROIs) shown below and white
931 arrows indicate YFP-A3G clustering at PM. Figure corresponds to Supplementary Movie
932 2. **(G)** Fixed cell images show Gag and *gagpol* mRNA (viral RNA genomes) accumulating
933 with YFP-A3G at the cell periphery. White arrows highlight cell-peripheral clusters of YFP-
934 A3G, Gag, and genome. (**H)** TSEM images showing virus particles clustering in the
935 extracellular space after budding from HeLa.YFP-A3G cells infected with either Vif+ or

936 Vifxx viruses. All scale bars in fluorescent images = 10μm and in TSEM = 100nm. Error
937 bars represent standard deviation of the mean. **(I)** Representative images from long-term
938 time-lapse imaging showing YFP-A3G, YFP-MOV10, and YFP-UPF1 upon HIV-1 Vifxx
939 and Vif+ infection. Arrows highlight PM clusters. Figure corresponds to Movie S3.

940

941 **Figure 2.** HIV-1 infection has little to no impact on P-bodies or stress granules. **(A)**
942 HeLa.YFP-TIA-1 cells showing steady-state distribution (H_20 vehicle, left) and
943 accumulation into SGs (magenta arrows) following arsenite treatment (right, Ars). **(B)**
944 Representative images from time-lapse imaging showing induction of SGs during
945 infection by RVA16 (MOI=10). Figure corresponds to Movie S4. **(C)** Time-lapse images
946 showing no effect on YFP-TIA-1 distribution following Vifxx CFP infection, quantified in
947 **(D)** for >400 HeLa.YFP-A3G (black bars) and HeLa.YFP-TIA-1 (gray bars) cells per
948 condition, combined from three independent experiments. **(E)** Time-lapse images
949 showing no effect on CFP-DCP1A following Vifxx mCh infection, quantified in **(F)** for 30
950 cells from 3 movies at ~18 hpi (YFP-A3G, black bars; CFP-DCP1A, white bars). **(G)**
951 HeLa.YFP-A3G infected with Vifxx CFP and treated with Ars to induce SGs at 24 hpi and
952 quantified in **(H)** for >100 infected cells from three independent experiments. Magenta
953 arrows highlight SGs present in infected cells. **(I)** Simultaneous FISH/IF to detect *gagpol*
954 mRNA and Gag show HIV RNA genomes accumulating in SGs in HIV infected cells
955 following Ars treatment. Magenta arrows highlight SGs present in infected cells. All scale
956 bars in fluorescent images = 10μm. Error bars represent standard deviation of the mean.

957

958 **Figure 3.** HIV-1 RNA genomes but not Gag regulate A3G subcellular localization. **(A)** and
959 **(C)** Schematics of Vif+ and Vifxx two-color self-tagging viruses encoding Gag-CFP,
960 24xMSL, and MS2-RFP. **(B)** and **(D)** Time-lapse images of cells expressing Vif+ and Vifxx
961 two-color HIV virus showing nuclear export of MS2-RFP tagged genomes, YFP-A3G
962 degradation (Vif+ in **(B)**) or localization with MS2-RFP (Vifxx in **(D)**), and Gag-CFP
963 expression and accumulation in virus particles at the PM (white arrows). Figure
964 corresponds to Movies S4 and S5. **(E)** and **(F)** Quantification of YFP-A3G degradation
965 and MS2-RFP cytoplasmic accumulation **(E)** and Gag-CFP expression **(F)** in single cells
966 during expression of Vif+ two-color HIV-1. Analysis includes cells that could be tracked
967 for at least 17 h (1 image/hour) extracted from three independent experiments (*n*=31).
968 Black lines highlight the ~3 h window of YFP-A3G degradation. T=0 represents onset of
969 MS2-RFP expression. **(G)** Schematic of "genome only" and "Gag only" RNA constructs
970 used for fluorescence recovery after photobleaching (FRAP) analysis. **(H)** Representative
971 images from prior to (top) and after (before) photobleaching regions of HeLa.YFP-A3G
972 cells expressing HIV-1 genomes in the absence of Gag ("genome only" condition). White
973 dashed circles represent regions of targeted photobleaching. **(I)** Quantification of YFP-
974 A3G FRAP experiments and zoomed inset of time period over first 80 seconds after
975 photobleaching. Incomplete recovery is best explained by an immobilized fraction of YFP-
976 A3G. All scale bars in fluorescent images = 10μm. Error bars represent standard deviation
977 of the mean.

978 **Figure 4.** Viral RNA genome-A3G interactions are sufficiently strong to redistribute A3G
979 to unnatural subcellular locales. **(A)** Schematic description of the new In Cell RNA-protein
980 Interaction Protocol (IC-IP). **(B)** Schematic of MS2-iRFP constructs used for "targeting"

981 (top) and representative images of MS2-iRFP and YFP-A3G localization in the absence
982 of mRNAs encoding MSL cassettes. White arrows point to characteristic subcellular
983 targets of Src- (vesicles) or Lifeact- (filamentous actin) MS2-iRFP. **(C)** Schematic of the
984 IC-IP RNA bait used to study YFP-A3G; a Vifxx two-color self-tagging HIV genome. **(D)**
985 Representative images showing "Free" MS2-iRFP-NLS, YFP-A3G, and Gag-CFP
986 accumulating at PM-adjacent assembly sites consistent with the native assembly pathway
987 (top). (Middle) Src-MS2-iRFP accumulating at intracellular/perinuclear vesicles and
988 recruiting MS2-RFP-tagged RNA genomes, YFP-A3G, and Gag-CFP to these vesicles.
989 (Bottom) Lifeact-MS2-iRFP accumulating at F-actin filaments and recruiting MS2-RFP-
990 tagged RNA genomes, YFP-A3G, and Gag-CFP to these F-actin filaments. Regions of
991 interest (ROIs) show YFP-A3G signal in dashed white boxes with arrows highlighting
992 YFP-A3G localization at assembly sites (top) or genome-dependent re-localization to
993 vesicles (middle), or linear F-actin filaments (bottom). **(E)** Single cell quantification of YFP-
994 A3G localization phenotypes (n = > 90 cells per condition) in the presence of NLS, Src-,
995 and Lifeact-MS2 targeting constructs. Asterisks demarcate p-values as follows: *≤0.05,
996 **≤0.005, ***≤0.0005. **(F)** Percentages of total YFP-A3G per cell fluorescence (IntDen)
997 re-localized by Src- or Lifeact-MS2 constructs for a subset of cells per condition (n > 6).
998 All scale bars in fluorescent images = 10μm, except for YFP-A3G ROIs (1μm). Error bars
999 represent standard deviation of the mean.

1000

1001 **Figure 5.** Recruitment of YFP-A3G and MOV10 is selective for HIV-1 RNA genomes,
1002 Gag-independent, and occurs long before the onset of virus particle assembly. **(A)** and
1003 **(C)** Schematics of "genome only" and "Gag only" IC-IP bait constructs, respectively, used

1004 in these experiments. **(B)** Representative images showing co-distribution of MS2-RFP
1005 tagged RNA genomes and YFP-A3G under native expression conditions (top) vs.
1006 retargeting of YFP-A3G to intracellular vesicles when RNA genomes are tethered to
1007 vesicles by Src-MS2-iRFP (bottom). **(D)** Representative images showing specificity,
1008 wherein Src-MS2-RFP has no effect on YFP-A3G in the presence of "Gag-only" codon-
1009 optimized IC-IP bait mRNAs (white arrow). CFP (blue) channel confirms high-level "Gag-
1010 only" mRNA expression based on Gag-CFP synthesis. **(E)** Time-lapse images of cells
1011 expressing MS2-RFP-tagged HIV-1 genomes in the absence of Gag ("genome only"
1012 construct) and being retargeted by Src-MS2-iRFP over a period of 4 hours. T=0
1013 represents the first detection of the MS2-RFP genome proxy. Arrow shows accumulation
1014 of YFP-A3G at Src-MS2-iRFP+ vesicles as early as 2 hours after the onset of MS2-RFP
1015 expression. All scale bars in fluorescent images = 10μm. **(F)** Representative IC-IP images
1016 of HIV genomes and the indicated RBPs retargeted by Lifeact-MS2-iRFP. ROIs *i-iv* shown
1017 below in black and white show re-localization of YFP-A3G and YFP-MOV10 to F-actin
1018 filaments by HIV-1 genomes even in the absence of Gag ("genome only). The dRRE
1019 control expressed an HIV-1 genome wherein the Rev response element (RRE) is deleted
1020 to prevent genome export from the nucleus (see MS2-RFP signal). **(G)** Unbiased
1021 quantification of IC-IP interactions based on colocalization analysis of Lifeact-MS2-iRFP
1022 targeter and YFP-A3G, YFP-MOV10, or YPF-UPF1 RBP prey for the indicated RNA baits.
1023 Non-thresholded Pearson's coefficients were calculated, comparing targeter & RBP
1024 overlap from ROIs for ~10 cells chosen at random per conditions. Error bars represent
1025 standard deviation from the mean. Asterisks demarcate p-values as follows: *≤0.05,
1026 **≤0.005, ***≤0.0005.All scale bars in fluorescent images = 10μm.

1027

1028 **Figure 6.** Membrane-targeted APOBEC3G recruits HIV-1 RNA genomes and can inhibit
1029 virus particle production. **(A)** Schematic of "Reciprocal IC-IP" experimental set-up to test
1030 if Src-YFP-A3G recruits viral genomes to intracellular membranes. **(B)** Schematic of Vifxx
1031 2-color genome and accumulation of MS2-RFP-tagged genomes and Gag-CFP at
1032 intracellular vesicles (white arrows) when co-expressed with Src-YFP-A3G. **(C)** As for (B),
1033 but using a "Genome only" construct co-expressed with Src-CFP-A3G in YFP-A3G cells.
1034 **(D)** Schematic of Vifxx Luc HIV infectious single-cycle (no MSL) virus used to infect
1035 HeLa.Src-YFP-A3G cells and representative images of FISH/IF detecting *gag-pol* mRNA
1036 and Gag p-24, respectively. White arrows highlight sites where Src-YFP-A3G recruited
1037 *bona fide* HIV RNA genomes to vesicles. **(E)** Western blot showing dose-dependent
1038 inhibition of HIV virus particle assembly and production from HEK293T cells transfected
1039 to co-express Vifxx two-color HIV-1 with Src-MS2-YFP (lanes 1 and 2), YFP-A3G (lane
1040 3) or Src-YFP-A3G (lanes 4 and 5). Graph shows relative virus particle release efficiency
1041 measured as the relative ratio of Gag in virus-like particles (VLPs) to Gag in cellular
1042 lysates ("release factor") quantified from three independent experiments. All scale bars in
1043 fluorescent images = 10μm. Error bars represent standard deviation of the mean.

1044

1045 **Figure 7.** Cytoplasmic A3G-genome interactions promote consistent per virion delivery
1046 of A3G into progeny virions. **(A)** Schematics of constructs used for our single virion
1047 analysis (SVA) studies. **(B)** Western blot confirming expression and packaging of YFP-
1048 A3G only for Vifxx and Gag-only conditions. **(C)** Representative images of single
1049 fluorescent virions harvested from our HEK293T.YFP-A3G cell line (see Figure 1C).

1050 Scale bar = 500nm. **(D)** Quantification of SVA for each of the four constructs showing
1051 percent of virions with MS2-RFP signal (pink) and YFP-A3G (green). Error bars represent
1052 standard deviation of the mean (*n* > 13,000 virions per condition). **(E)** Relative YFP-A3G
1053 signal per virion or virus-like particle derived from Vifxx two-color or COGag conditions.
1054 Relative values are normalized to the mean value for Vifxx with means (solid lines) and
1055 25th and 75th quartiles (dashed lines) indicated.

1056 **SUPPLEMENTAL FIGURE LEGENDS**

1057 **Figure S1.** HIV-1 infection alters shifts MOV10 but not UPF1 from the cytoplasm to the
1058 plasma membrane. **(A)** Overexpression screen of YFP-tagged RBPs. 293T cells were
1059 transfected to generate PR-minus HIV-1 VLPs with co-expression of the indicated YFP-
1060 RBP proteins (or YFP as a control, lane 12), with lysates and supernatants harvested at
1061 48 h. GAPDH served as a loading control. (**B-D).** Representative images from time-lapse
1062 imaging showing relocalization of YFP-A3G and YFP-MOV10 but not YFP-UPF1 during
1063 infection with HIV-1 Vifxx CFP virus. Black and white ROIs highlight >1 μm clusters of
1064 YFP-A3G and YFP-MOV10 enriched at the plasma membrane of infected cells at later
1065 time points, not observed for YFP-UPF1. **(E)** Select images from time lapse videos
1066 showing YFP-MOV10 clusters at the plasma membrane both in the presence and
1067 absence of Vif expression. Size bars represent 10 μm.

1068

1069 **Figure S2.** Cellular RBPs are recruited by HIV-1 RNA genomes. (A) Representative
1070 images showing co-distribution of MS2-RFP tagged RNA genomes (pink) and YFP-RBPs
1071 (green) under native expression conditions. CFP-DCP1A is shown in blue. Top panel
1072 shows images from transfections in cells stably expressing YFP-RBPs. Bottom panel
1073 shows images from co-transfection of YFP-RBPs with self-tagging HIV genome. (B)
1074 Representative images showing co-distribution of MS2-RFP tagged RNA genomes (pink)
1075 and YFP-RBPs (green) during retargeting to intracellular vesicles when RNA genomes
1076 are tethered to vesicles by Src-MS2-iRFP. Arrows indicate intense recruitment of MOV10
1077 and (to a lesser degree) PABPc1. Other RBPs show minimal (XPO1, UPF1, DDX3) or no
1078 (RPL9, TIA-1, DCP1A, CBP80) recruitment to Src-MS2-iRFP retargeted HIV genomes.

1079 **SUPPLEMENTAL MOVIE LEGENDS**

1080 **Movie S1. Time-lapse imaging of HeLa-.YFP-A3G cells infected with Vif+ HIV-1/CFP**
1081 **virus.** Multi-channel images of HeLa.YFP-A3G cells were acquired every 60 minutes for
1082 49h after infection. In the highlighted cell, viral gene expression (cyan) is detected ~16hpi
1083 with YFP-A3G (green) degradation at 21hpi. Cell rounds at 28 hpi consistent with Vif-
1084 induced G2/M cell cycle arrest.

1085

1086 **Movie S2. Time-lapse imaging of HeLa.YFP-A3G cells infected with Vifxx HIV-1/CFP**
1087 **virus.** Multi-channel images were acquired every 60 minutes for 49h after infection. In the
1088 highlighted cell, viral gene expression (cyan) is detected ~19hpi with detection of YFP-
1089 A3G (green) at virus particles (arrows) starting at ~25hpi. An example of a transfer event
1090 wherein a large cluster of YFP-A3G+ virus particles is released from an infected cell is
1091 highlighted (arrows) at 32-36hpi.

1092

1093 **Movie S3. Time-lapse imaging of HeLa.YFP-MOV10 and HeLa-YFP-UPF1 cells**
1094 **infected with Vifxx HIV-1/CFP virus.** Multi-channel images were acquired every 60
1095 minutes for 96hpi with Vif+ or Vifxx HIV-1/CFP viruses. A 72h time window is shown,
1096 initiating ~3 hours prior to the onset of viral gene expression (cyan). Vif+ HIV-1 degrades
1097 YFP-A3G (top left panel, green) while Vifxx HIV-1 triggers relocalization of YFP-A3G
1098 (bottom left panel, green) to plasma membrane clusters (arrows). YFP-MOV10 (central
1099 panels, green) is re-localized to plasma membrane clusters (arrows) with or without Vif

1100 expression. YFP-UPF1 was largely unaffected by HIV-1 in the presence or absence of
1101 Vif, but with some rare instances of cytoplasmic granule formation.

1102

1103 **Movie S4. Time-lapse imaging of HeLa.YFP-TIA-1 cells infected with Rhinovirus**
1104 **A16.** Multi-channel images were acquired every 30 minutes after addition of RVA16
1105 (MOI~10). The first instances of SG formation (YFP-TIA-1 in green) are evident at ~11hpi.

1106

1107 **Movie S5. Time-lapse imaging of HeLa.YFP-A3G cells expressing the two-color Vif+**
1108 **Gag-CFP/MS2-RFP HIV-1 reporter virus.** Multi-channel images were acquired every 60
1109 minutes for 24h beginning ~4h post-transfection. Left panel shows genome tracked using
1110 MS2-RFP (magenta), with nuclear export detected at T=4h just prior to the onset of Gag-
1111 CFP (cyan) expression (right panel) and YFP-A3G (green) degradation (center panel).

1112

1113 **Movie S6. Time-lapse imaging of HeLa.YFP-A3G cells expressing the two-color**
1114 **Vifxx Gag-CFP/MS2-RFP HIV-1 reporter virus.** Multi-channel images were acquired
1115 every 60 minutes for 24 hours beginning ~4 hours post-transfection. Left panel shows
1116 genome tracked using MS2-RFP (magenta), with nuclear export detected at T=6h just
1117 prior to the onset of Gag-CFP (cyan) expression (right panel) and co-accumulation of
1118 YFP-A3G (green, center panel) with genome (MS2-RFP) and Gag-CFP at the plasma
1119 membrane (at putative sites of virus particle assembly).

1120

1121 **Movie S7. Time-lapse imaging of HeLa.YFP-A3G cells co-expressing "genome**
1122 **only" MS2-RFP HIV-1 reporter virus with the Src-MS2-iRFP targeter (orange).** Multi-
1123 channel images were acquired every 60 minutes for 15h starting ~4h post-transfection.
1124 MS2-RFP tracked genomes (magenta, central panel) are first observed at T=0, with both
1125 genomes and YFP-A3G (green, right panel) immediately recruited to perinuclear vesicles,
1126 co-localizing with the Src-MS2-iRFP targeter (yellow, left panel). Video demonstrates that
1127 genomes have marked effects on YFP-A3G trafficking in the cytosol even at the earliest
1128 time points post-genome nuclear export.

Figure 1

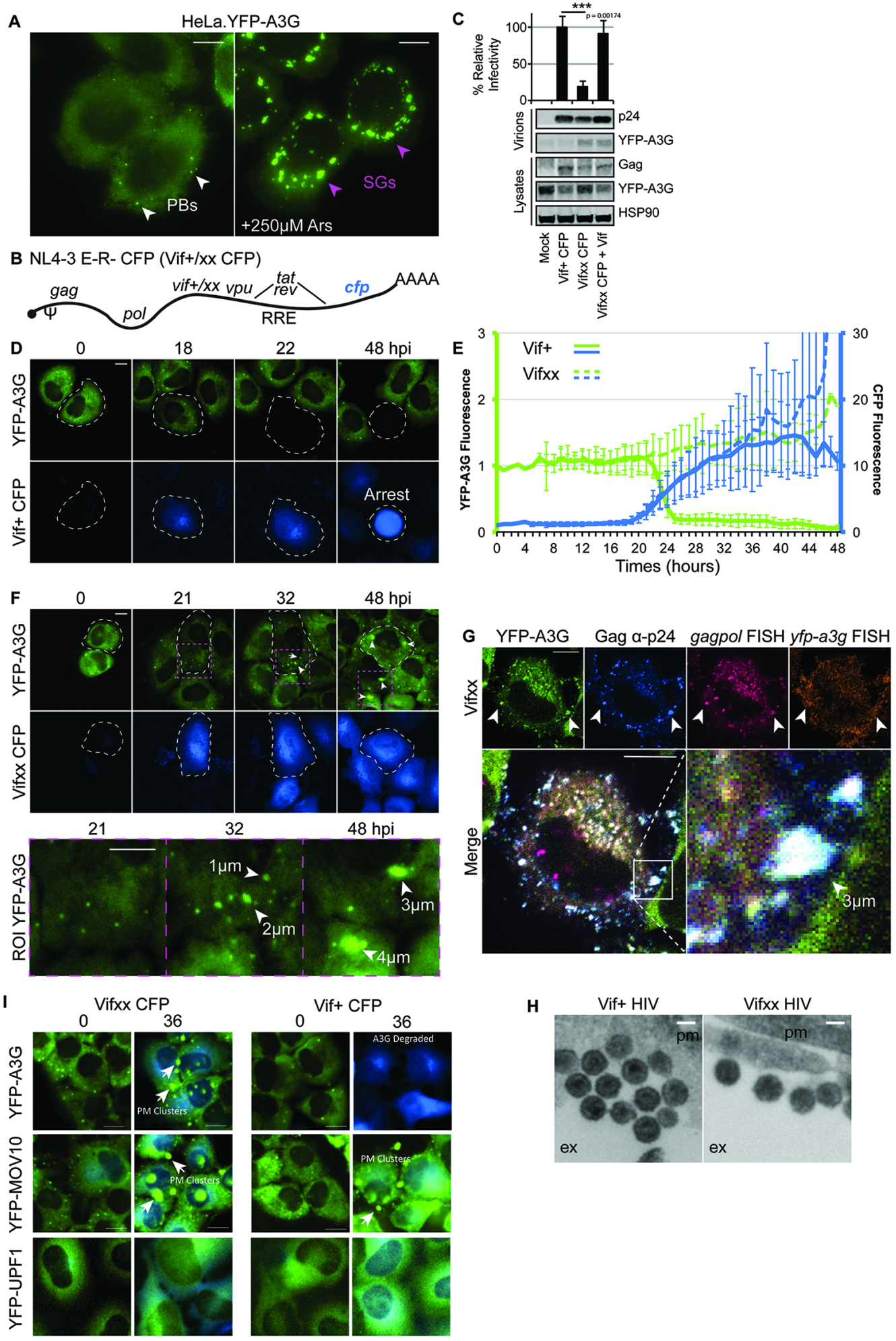
A
HeLa.YFP-A3G
PBs
SGs
+250μM Ars
B NL4-3 E-R- CFP (Vif+/xx CFP)
gag
Ψ
pol
vif+/xx vpu
tat
rev
RRE
cfp
AAAA
C
% Relative Infectivity
***
p = 0.00174
Virions
Lysates
p24
YFP-A3G
Gag
YFP-A3G
HSP90
Mock
Vif+ CFP
Vifxx CFP
Vifxx CFP + Vif
D
0
18
22
48 hpi
YFP-A3G
Vif+ CFP
Arrest
E
Vif+
Vifxx
YFP-A3G Fluorescence
CFP Fluorescence
Times (hours)
F
0
21
32
48 hpi
YFP-A3G
Vifxx CFP
ROI YFP-A3G
1μm
2μm
3μm
4μm
G
YFP-A3G
Gag α-p24
gagpol FISH
yfp-a3g FISH
Vifxx
Merge
3μm
I
Vifxx CFP
Vif+ CFP
0
36
A3G Degraded
YFP-A3G
YFP-MOV10
YFP-UPF1
PM Clusters
H
Vif+ HIV
Vifxx HIV
pm
ex

Figure 2

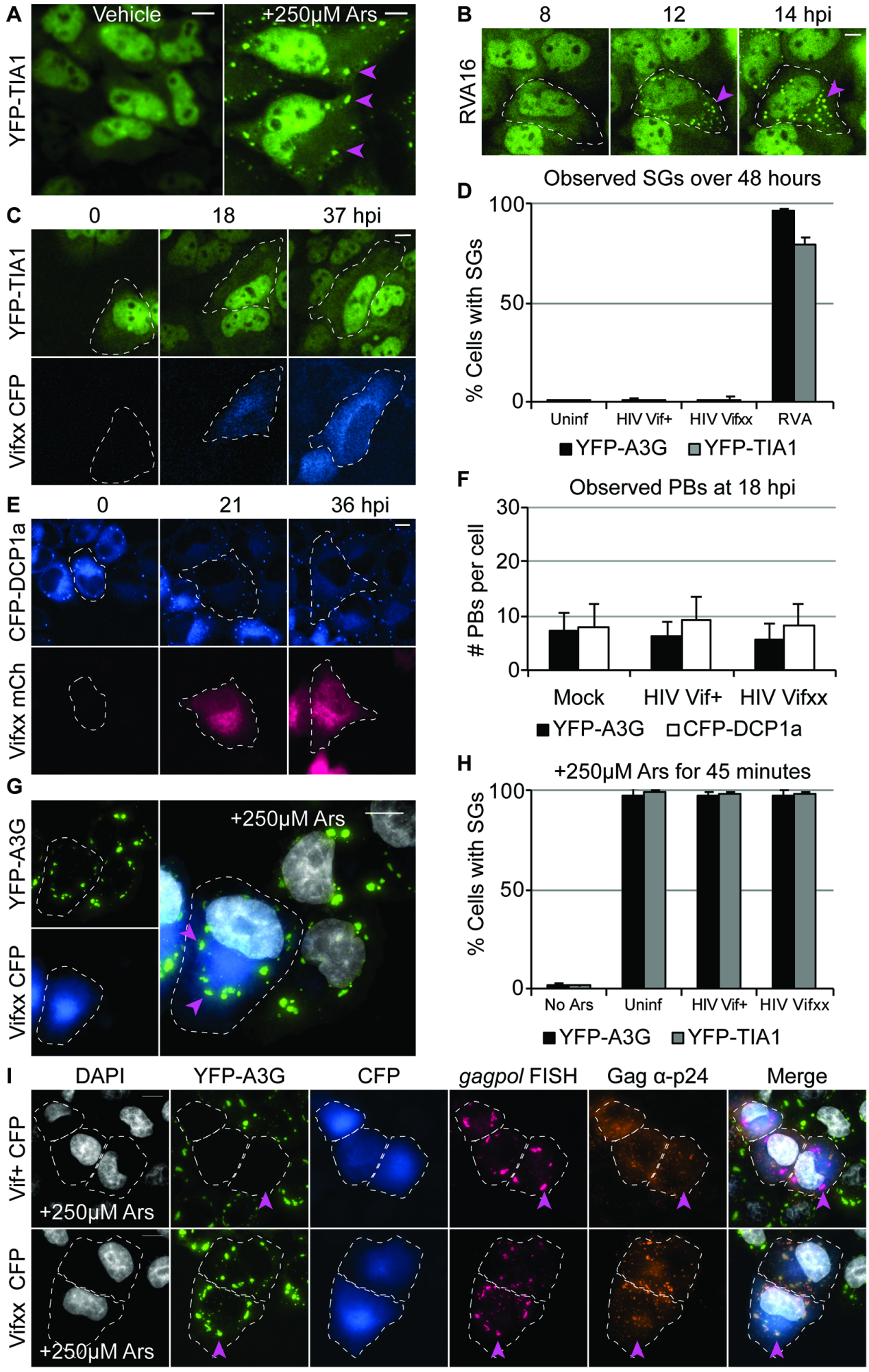
A
Vehicle
+250μM Ars
YFP-TIA1
B
8
12
14 hpi
RVA16
C
0
18
37 hpi
YFP-TIA1
Vifxx CFP
D
Observed SGs over 48 hours
% Cells with SGs
100
50
0
Uninf
HIV Vif+
HIV Vifxx
RVA
YFP-A3G
YFP-TIA1
E
0
21
36 hpi
CFP-DCP1a
Vifxx mCh
F
Observed PBs at 18 hpi
PBs per cell
30
20
10
0
Mock
HIV Vif+
HIV Vifxx
YFP-A3G
CFP-DCP1a
G
YFP-A3G
Vifxx CFP
+250μM Ars
H
+250μM Ars for 45 minutes
% Cells with SGs
100
50
0
No Ars
Uninf
HIV Vif+
HIV Vifxx
YFP-A3G
YFP-TIA1
I
DAPI
YFP-A3G
CFP
gagpol FISH
Gag α-p24
Merge
Vif+ CFP
+250μM Ars
Vifxx CFP
+250μM Ars

Figure 3

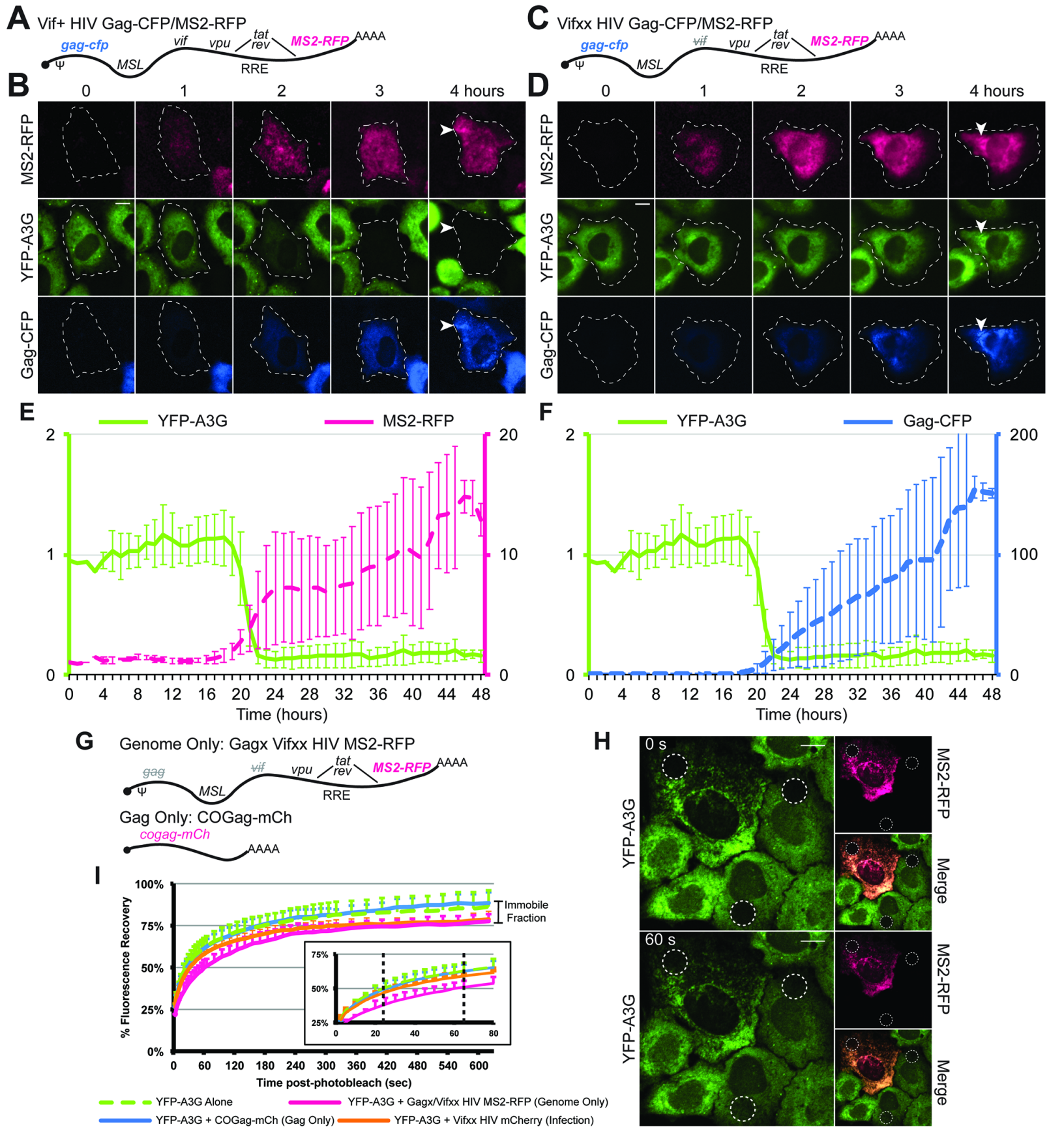
A
Vif+ HIV Gag-CFP/MS2-RFP
gag-cfp
Ψ
MSL
vif
vpu
tat
rev
RRE
MS2-RFP
AAAA
B
0
1
2
3
4 hours
MS2-RFP
YFP-A3G
Gag-CFP
C
Vifxx HIV Gag-CFP/MS2-RFP
D
E
YFP-A3G
MS2-RFP
Time (hours)
F
Gag-CFP
G
Genome Only: Gagx Vifxx HIV MS2-RFP
gag
Gag Only: COGag-mCh
cogag-mCh
H
0 s
60 s
Merge
I
% Fluorescence Recovery
Time post-photobleach (sec)
Immobile Fraction
YFP-A3G Alone
YFP-A3G + Gagx/Vifxx HIV MS2-RFP (Genome Only)
YFP-A3G + COGag-mCh (Gag Only)
YFP-A3G + Vifxx HIV mCherry (Infection)

Figure 4

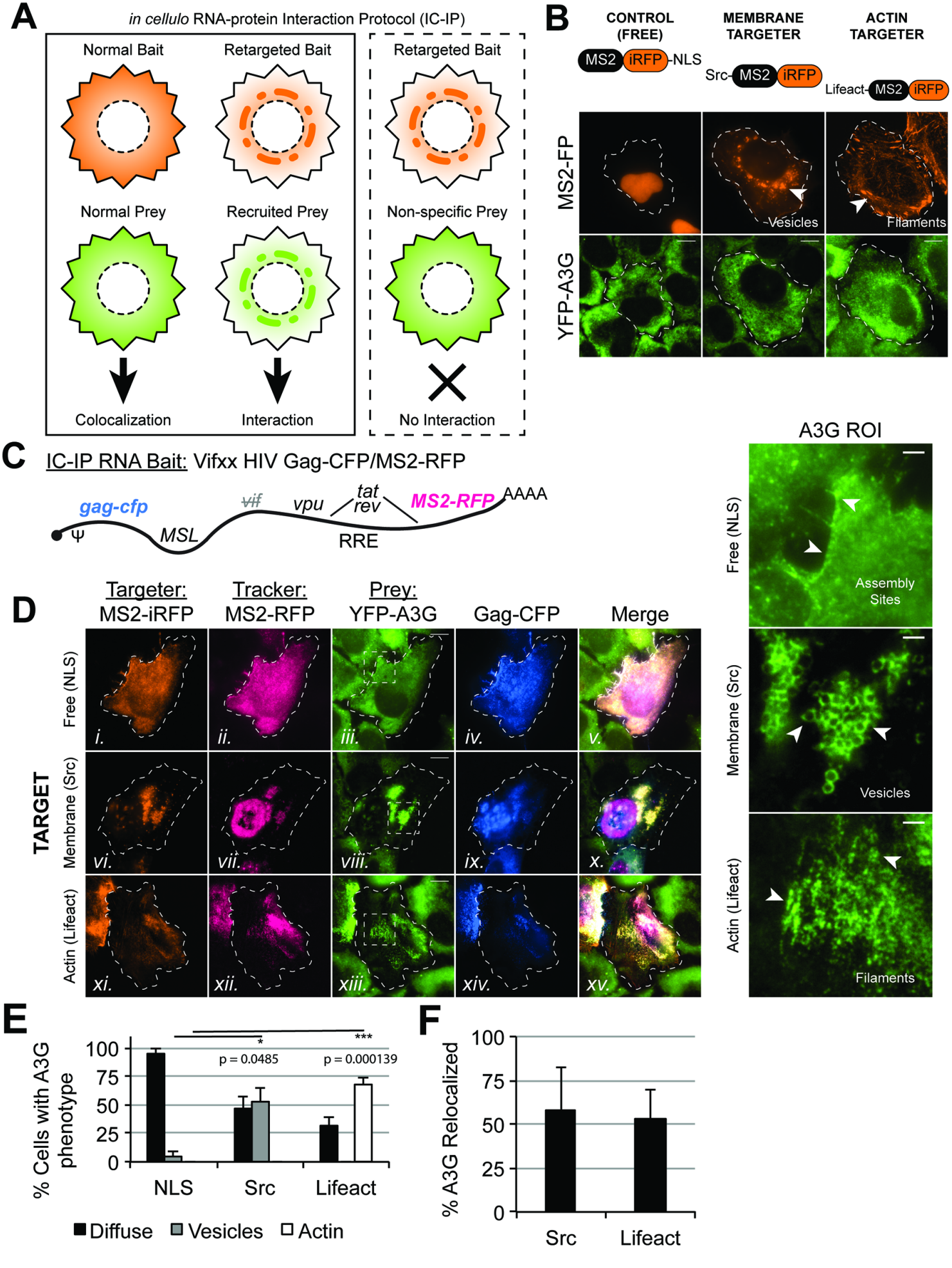
A
in cellulo RNA-protein Interaction Protocol (IC-IP)
Normal Bait
Retargeted Bait
Retargeted Bait
Normal Prey
Recruited Prey
Non-specific Prey
Colocalization
Interaction
No Interaction
B
CONTROL (FREE)
MEMBRANE TARGETER
ACTIN TARGETER
MS2
iRFP
-NLS
Src-
Lifeact-
MS2-FP
YFP-A3G
Vesicles
Filaments
C
IC-IP RNA Bait: Vifxx HIV Gag-CFP/MS2-RFP
gag-cfp
vif
vpu
tat
rev
MS2-RFP
AAAA
Ψ
MSL
RRE
A3G ROI
Free (NLS)
Assembly Sites
Membrane (Src)
Vesicles
Actin (Lifeact)
Filaments
D
Targeter: MS2-iRFP
Tracker: MS2-RFP
Prey: YFP-A3G
Gag-CFP
Merge
TARGET
Free (NLS)
Membrane (Src)
Actin (Lifeact)
i.
ii.
iii.
iv.
v.
vi.
vii.
viii.
ix.
x.
xi.
xii.
xiii.
xiv.
xv.
E
% Cells with A3G phenotype
100
75
50
25
0
*
p = 0.0485
***
p = 0.000139
NLS
Src
Lifeact
Diffuse
Vesicles
Actin
F
% A3G Relocalized
100
75
50
25
0
Src
Lifeact

Figure 5

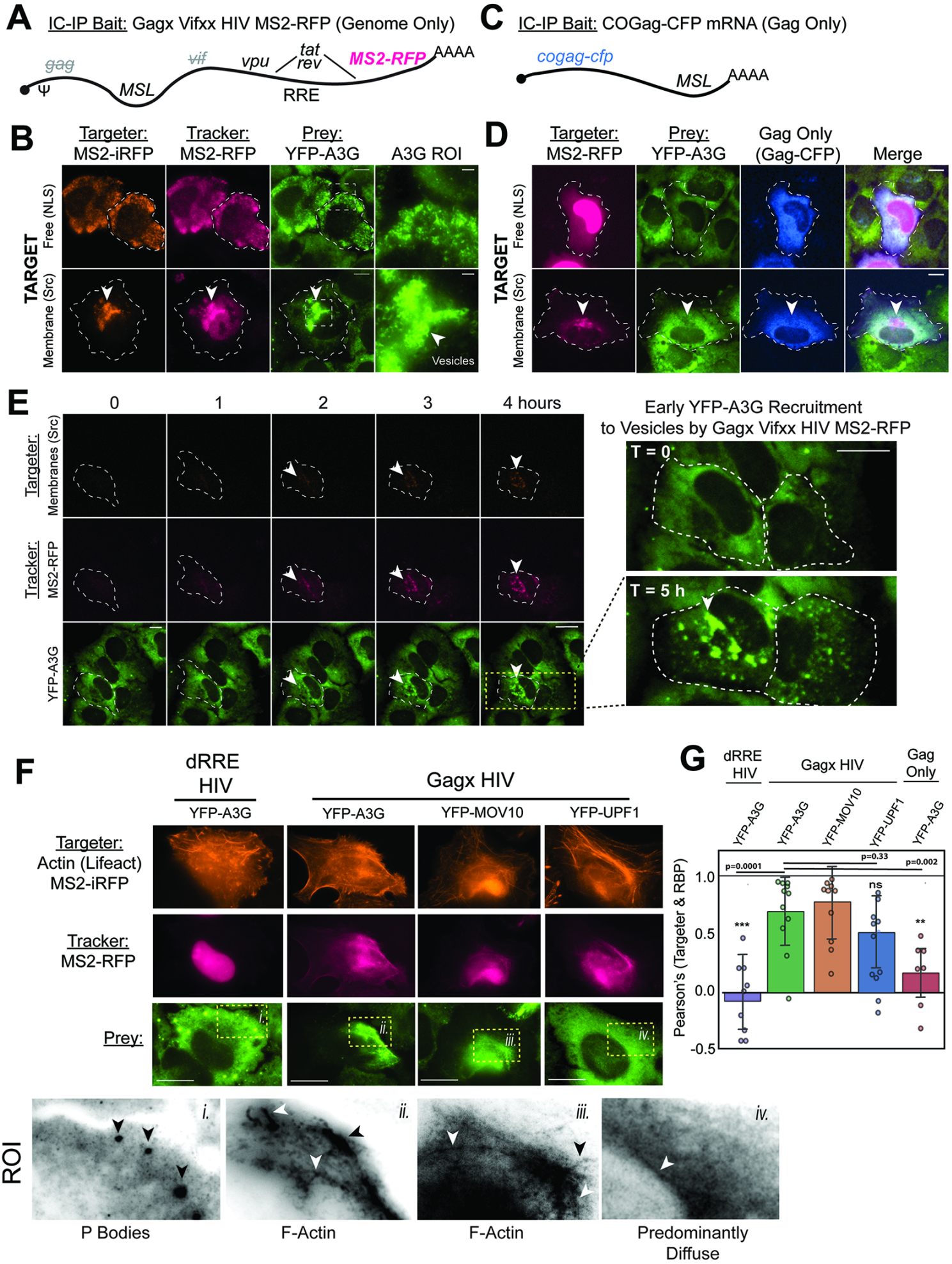
A
IC-IP Bait: Gagx Vifxx HIV MS2-RFP (Genome Only)
gag
vif
vpu
tat
rev
MS2-RFP
AAAA
ψ
MSL
RRE
C
IC-IP Bait: COGag-CFP mRNA (Gag Only)
cogag-cfp
MSL
AAAA
B
Targeter: MS2-iRFP
Tracker: MS2-RFP
Prey: YFP-A3G
A3G ROI
TARGET
Free (NLS)
Membrane (Src)
Vesicles
D
Targeter: MS2-RFP
Prey: YFP-A3G
Gag Only (Gag-CFP)
Merge
E
0
1
2
3
4 hours
Targeter: Membranes (Src)
Tracker: MS2-RFP
YFP-A3G
Early YFP-A3G Recruitment to Vesicles by Gagx Vifxx HIV MS2-RFP
T = 0
T = 5 h
F
dRRE HIV
Gagx HIV
YFP-A3G
YFP-A3G
YFP-MOV10
YFP-UPF1
Targeter: Actin (Lifeact) MS2-iRFP
Tracker: MS2-RFP
Prey:
i.
ii.
iii.
iv.
G
dRRE HIV
Gagx HIV
Gag Only
YFP-A3G
YFP-A3G
YFP-MOV10
YFP-UPF1
YFP-A3G
p=0.0001
p=0.33
p=0.002
***
ns
**
Pearson's (Targeter & RBP)
1.0
0.5
0.0
-0.5
ROI
i.
ii.
iii.
iv.
P Bodies
F-Actin
F-Actin
Predominantly Diffuse

Figure 6

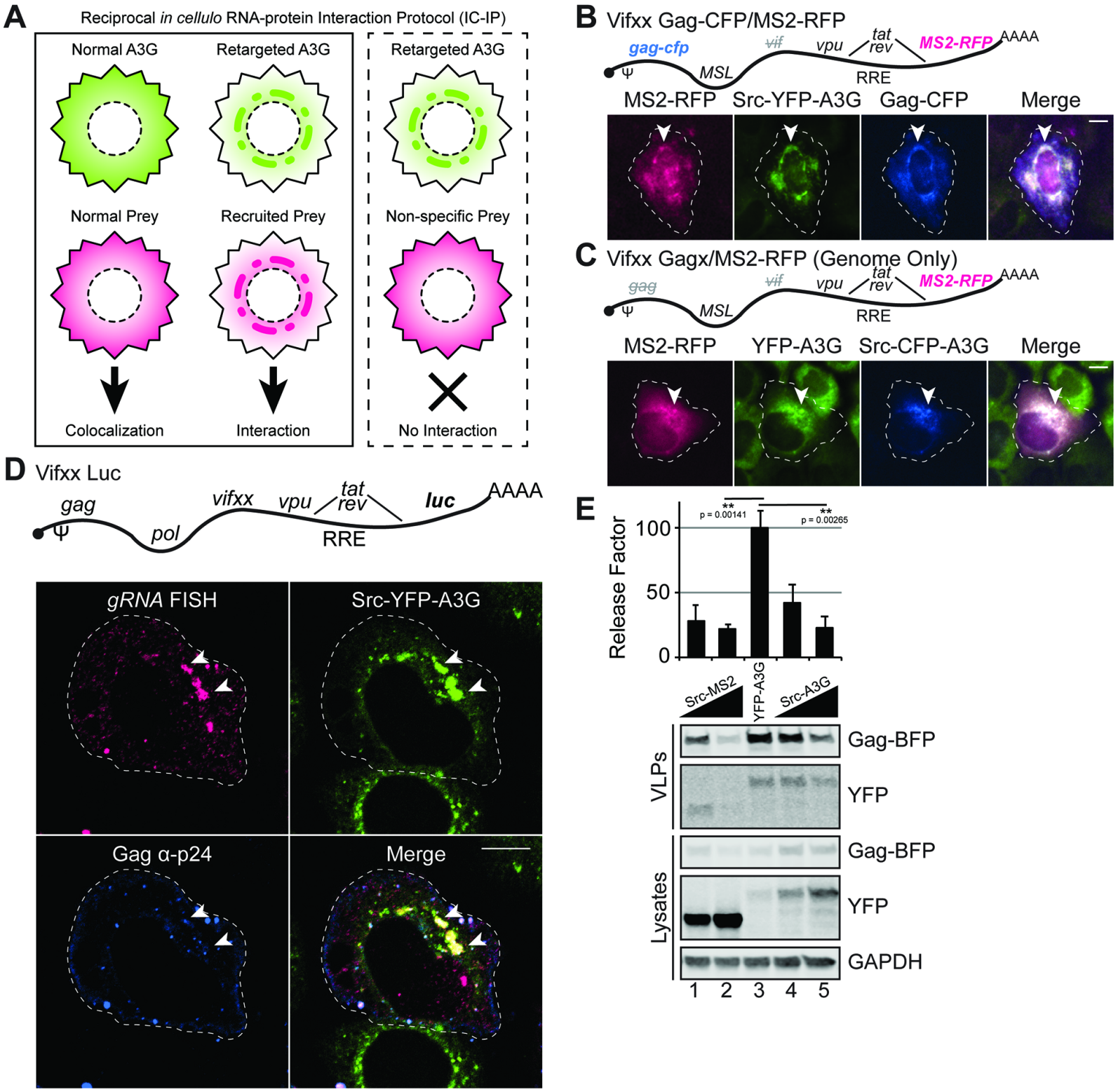
A
Reciprocal in cellulo RNA-protein Interaction Protocol (IC-IP)
Normal A3G
Retargeted A3G
Retargeted A3G
Normal Prey
Recruited Prey
Non-specific Prey
Colocalization
Interaction
No Interaction
B
Vifxx Gag-CFP/MS2-RFP
gag-cfp
vif
vpu
tat
rev
MS2-RFP
AAAA
Ψ
MSL
RRE
MS2-RFP
Src-YFP-A3G
Gag-CFP
Merge
C
Vifxx Gagx/MS2-RFP (Genome Only)
gag
vif
vpu
tat
rev
MS2-RFP
AAAA
Ψ
MSL
RRE
MS2-RFP
YFP-A3G
Src-CFP-A3G
Merge
D
Vifxx Luc
gag
Ψ
pol
vifxx
vpu
tat
rev
luc
AAAA
RRE
gRNA FISH
Src-YFP-A3G
Gag α-p24
Merge
E
Release Factor
100
50
0
**
p = 0.00141
**
p = 0.00265
Src-MS2
YFP-A3G
Src-A3G
VLPs
Gag-BFP
YFP
Lysates
Gag-BFP
YFP
GAPDH
1
2
3
4
5

Figure 7

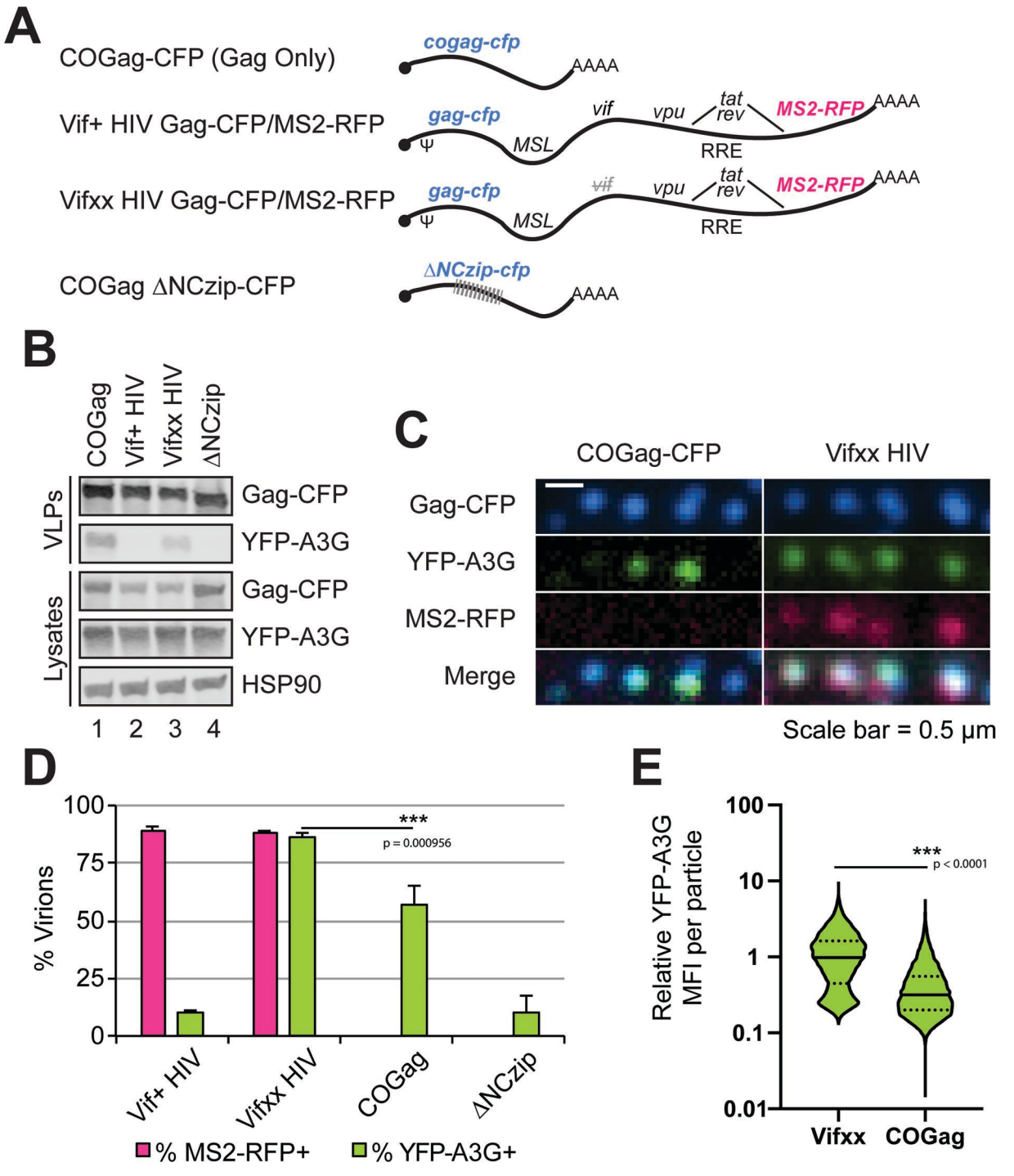
A
COGag-CFP (Gag Only)
cogag-cfp
AAAA
Vif+ HIV Gag-CFP/MS2-RFP
gag-cfp
Ψ
MSL
vif
vpu
tat
rev
RRE
MS2-RFP
AAAA
Vifxx HIV Gag-CFP/MS2-RFP
gag-cfp
Ψ
MSL
vif
vpu
tat
rev
RRE
MS2-RFP
AAAA
COGag ΔNCzip-CFP
ΔNCzip-cfp
AAAA
B
COGag
Vif+ HIV
Vifxx HIV
ΔNCzip
VLPs
Lysates
Gag-CFP
YFP-A3G
Gag-CFP
YFP-A3G
HSP90
1 2 3 4
C
COGag-CFP
Vifxx HIV
Gag-CFP
YFP-A3G
MS2-RFP
Merge
Scale bar = 0.5 µm
D
% Virions
100
75
50
25
0
***
p = 0.000956
Vif+ HIV
Vifxx HIV
COGag
ΔNCzip
% MS2-RFP+
% YFP-A3G+
E
Relative YFP-A3G MFI per particle
100
10
1
0.1
0.01
***
p < 0.0001
Vifxx
COGag

Figure S1

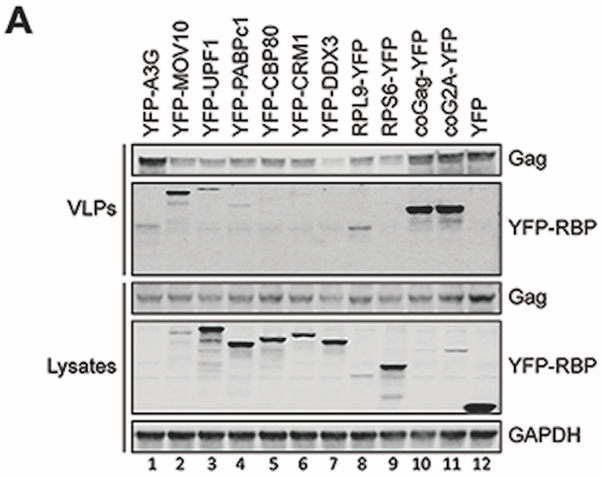
A
YFP-A3G
YFP-MOV10
YFP-UPF1
YFP-PABPc1
YFP-CBP80
YFP-CRM1
YFP-DDX3
RPL9-YFP
RPS6-YFP
coGag-YFP
coG2A-YFP
YFP
VLPs
Lysates
Gag
YFP-RBP
Gag
YFP-RBP
GAPDH
1 2 3 4 5 6 7 8 9 10 11 12

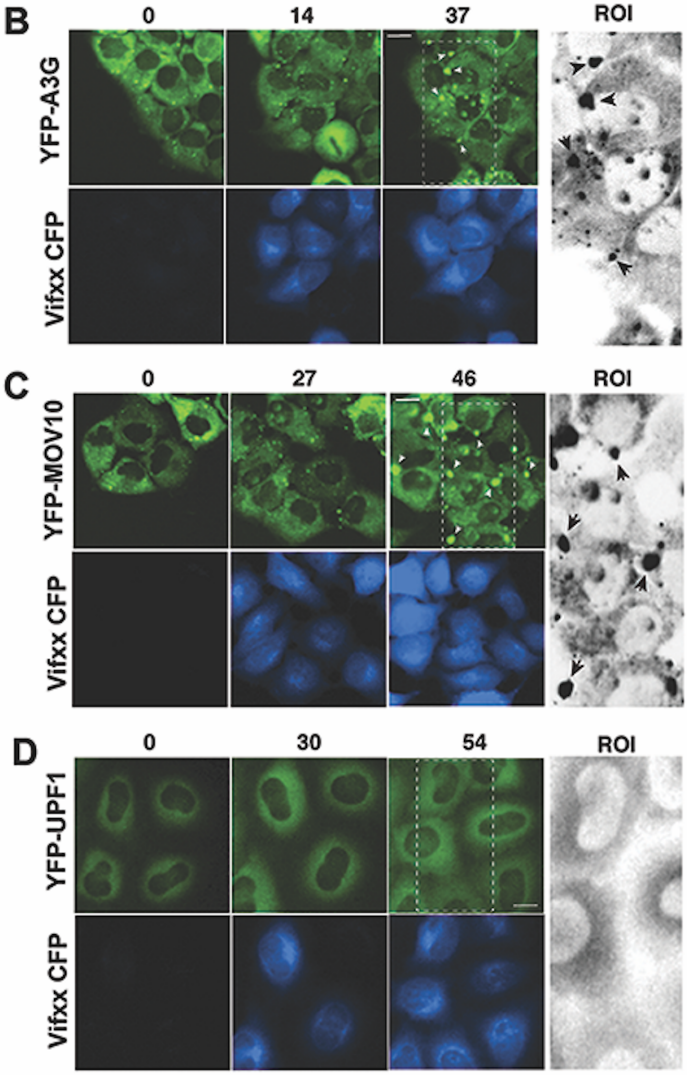
B
0
14
37
ROI
YFP-A3G
Vifxx CFP
C
0
27
46
ROI
YFP-MOV10
Vifxx CFP
D
0
30
54
ROI
YFP-UPF1
Vifxx CFP

Figure S2

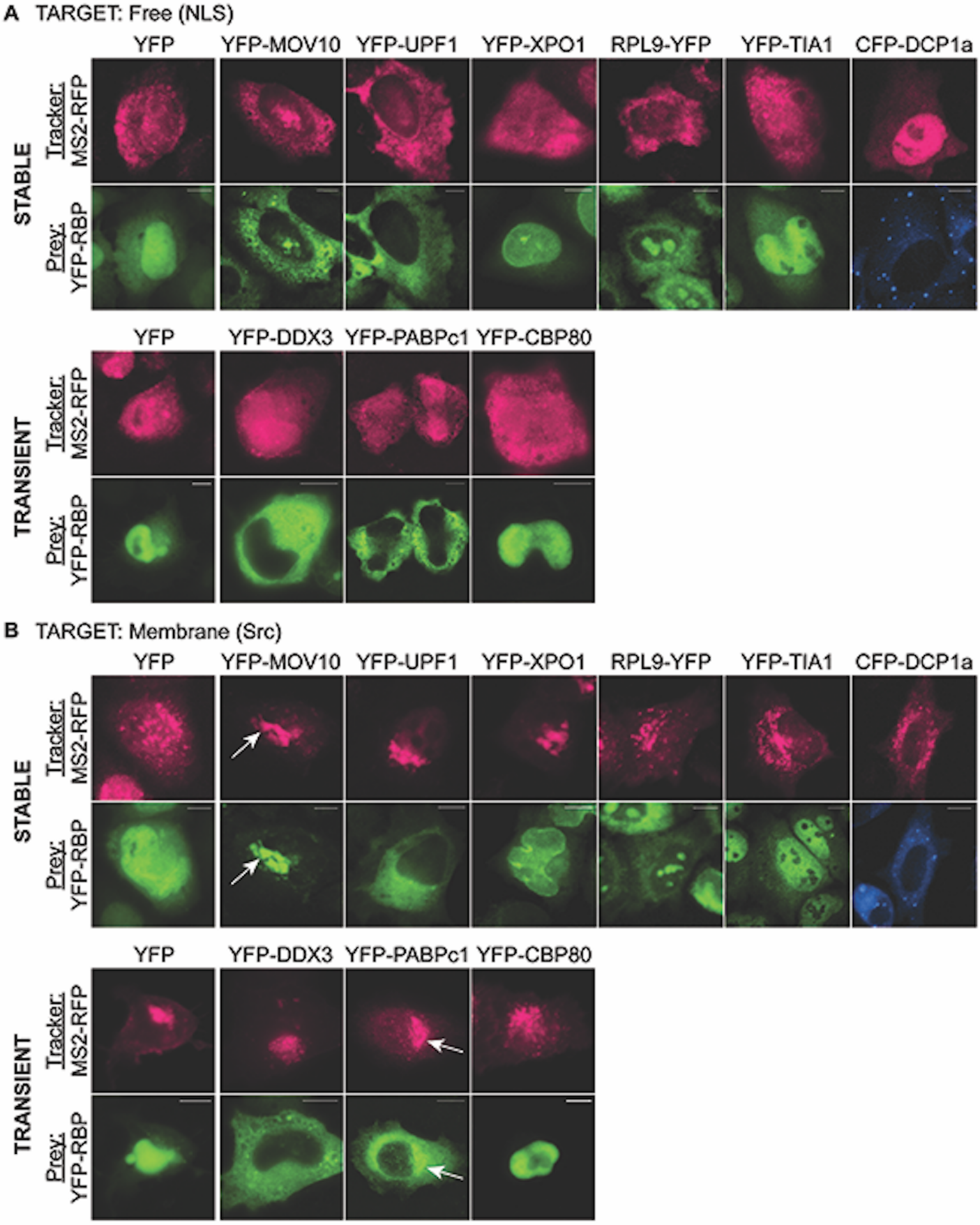
A TARGET: Free (NLS)
YFP
YFP-MOV10
YFP-UPF1
YFP-XPO1
RPL9-YFP
YFP-TIA1
CFP-DCP1a
STABLE
Tracker: MS2-RFP
Prey: YFP-RBP
YFP
YFP-DDX3
YFP-PABPc1
YFP-CBP80
TRANSIENT
Tracker: MS2-RFP
Prey: YFP-RBP
B TARGET: Membrane (Src)
YFP
YFP-MOV10
YFP-UPF1
YFP-XPO1
RPL9-YFP
YFP-TIA1
CFP-DCP1a
STABLE
Tracker: MS2-RFP
Prey: YFP-RBP
YFP
YFP-DDX3
YFP-PABPc1
YFP-CBP80
TRANSIENT
Tracker: MS2-RFP
Prey: YFP-RBP